Instrument Science Report STIS 2014-01

Summary of the STIS Cycle 19 Calibration Program

Julia Roman-Duval, Justin Ely, Alessandra Aloisi, Cristina Oliveira, Charles Proffitt, Svea Hernandez, Elena Mason, Paule Sonnentrucker, Michael Wolfe, Chris Long, Audrey DiFelice, Azalee K. Bostroem, Stephen Holland, Sean Lockwood, Colin Cox, Thomas Wheeler

November 26, 2014

ABSTRACT

We summarize the Cycle 19 calibration program for the Space Telescope Imaging Spectrograph (STIS) on the Hubble Space Telescope, covering the time period November 2011 through October 2012. We give an overview of the whole program, and status summaries for each of the individual proposals comprising the program.

1. Introduction

The Space Telescope Imaging Spectrograph (STIS) on the Hubble Space Telescope was repaired in May 2009. Cycle 19 was the third cycle of on-orbit post-repair STIS operations. The calibration program for this period resembles the typical calibration and monitoring programs of the mature STIS instrument prior to its failure in 2004, with fewer special calibrations than had been included in the Cycle 17 STIS calibration program. Cycle 19 observations commenced in November 2011 and ran through October 2012.

In this document we record and summarize the results of the individual calibration programs. Section 2 gives a summary and overview of the calibration program, which comprises 20 unique programs. All of these are regular programs to monitor and track instrument performance. However, one calibration program is devoted to obtaining data for a new spectroscopic flux calibration standard star. Section 3 of this document details results from individual programs. The Appendix lists reference files and documentation produced as a result of Cycle 18 calibration programs.

2. Overview of calibration proposals for Cycle 19

Table 1 summarizes the orbit allocation and usage during the regular and special Cycle 19 calibration program. No supplemental (special) calibration programs beyond those proposed as the initial calibration plan were required for STIS in this cycle.

Table 1. Summary of orbit allocation and use during Cycle 19 STIS calibration. The executed row includes all orbits, including those that failed and were then repeated.

	External Orbits		Internal+Parallel orbits	
	Regular	Special	Regular	Special
Allocated	21	0	1390+6[C]	0
Executed	21	0	1396	0
Withdrawn	0	0	0	0
Failed	0	0	10	0
Repeated	0	0	6	0

[C] Contingency orbits,

The calibration monitoring programs in Cycle 19 are essentially continuations of the monitoring programs from the previous cycle. These include programs which assess the stability of the CCD: its read out noise, spurious charge, charge transfer efficiency (CTE), and growth of hot pixels, and which also provide daily dark frames and bias frames for data processing and reduction. Other programs monitor the slit wheel repeatability, CCD and MAMA dispersion solutions, the MAMA focus, the MAMA fold distribution (i.e., the pulse-height distribution), and the sensitivity of both the CCD and MAMA detectors. For these programs, reference files are updated only as needed to maintain calibration within the required levels of accuracy.

Currently available reference files can be found at: www.stsci.edu/hst/observatory/crds/SIfileInfo/STIS/reftablequeryindex Other products resulting from the calibration program include STIS Instrument Science Reports (ISRs), STIS Technical Instrument Reports (TIRs), and updates to the STIS Instrument (IHB) and Data (DHB) Handbooks. Links to these documents can be found at: www.stsci.edu/hst/stis/documents. Note that TIRs are only available on the internal STScI web site. In order to retrieve TIRs a document request needs to be sent to: help@stsci.edu

Table 2 provides a high level summary of the calibration programs, noting specifically products and accuracy achieved. The first two columns give the Proposal ID and its title; columns 3 and 4 give the number of executed [allocated] orbits for each proposal, divided into external and internal orbits. Column 5 gives the frequency of visits for monitoring programs. Column 6 describes the resulting products. For several programs, regularly

updated reference files are produced. For many others, results are either posted on the web, or simply documented in Section 3 of this report. Column 7 gives the accuracy achieved by the calibration proposal. The last column of Table 2 notes the page in this ISR on which detailed information for that program can be found.

Table 2. Summary of Cycle 19 calibration programs. Further details can be found in the following sections. Some of the executed and allocated values differ due to some orbits failing.

	Title	**Orbits used Executed [Allocated]**		**Frequency**	**Products**	**Accuracy achieved**	**Page**
		External	**Internal**				
	CCD Monitors						
12740	CCD Performance Monitor	0	14 [14]	2x7	Reference file	5% (RN) <1% (G)	5
12741	CCD Dark Monitor Part I	0	364 [364]	364x1	Reference files	S/N~1.36	8
12742	CCD Dark Monitor Part II	0	368 [368]	368x1	Reference files	S/N~1.36	8
12743	CCD Bias and Readnoise Monitor Part I	0	182 [182]	182x1	Reference files	S/N~1.1-2.0	10
12744	CCD Bias and Readnoise Monitor Part II	0	184 [184]	184x1	Reference files	S/N~1.1-2.0	10
12765	CCD Hot Pixel Annealing	0	39 [39]	13x3	Webpage updates	See details in report	12
12766	CCD Spectroscopic Flats	0	19 [19]	various	Reported in this ISR	<1.1% residual scatter	14
12767	CCD Imaging Flats	0	8 [8]	various	Reported in this ISR	<0.2% residual scatter	16
12768	CCD Spectroscopic Dispersion Solution Monitor	0	3 [3]	3x1	ISR in prep	Zero-points vary with rms <0.35 pixel	18
12769	CCD Sparse Field CTE	0	$82+6^{H}$ [82]		Reported in this ISR	<1% for >200 e^-	22
12770	CCD Full Field Sensitivity	1 [1]	0	1x1	ISR	<1%	24
12771	Slit Wheel Repeatability	0	1 [1]	1x1	Reported in this ISR	Repeatable to 0.01 pixel	28
12772	CCD Spectroscopic Sensitivity Monitor	5 [5]	0	3x1/L,1x2/M	TDS reference file	<1% in rel. flux	29
	MAMA Monitors						
12773	MAMA Dispersion Solution	0	7 [7]	7x1	ISR in prep	Zero-points vary with rms <0.35 pixel	36
12774	MAMA Full Field Sensitivity	3 [3]	0	1x3	ISR	FUV-MAMA: <1% NUV-MAMA: <1%	42
12775	MAMA Spectroscopic Sensitivity and Focus Monitor and COS Observations of Geocoronal Lyman-alpha	12 [12]	0	3x1/L, 1x1/M, 4x2/E	TDS reference file + ISR	<2% /E, 0.2-0.5%/L,M	46
12776	FUV MAMA Dark Monitor	0	54 [54]	2x6	Reported in this ISR	5-10%	53
12776	NUV MAMA Dark Monitor	0	52 [52]	2/det/alt wks+	Reported in this ISR	5-10%	53
12777	MAMA NUV Flats	0	11 [11]	Odd cycles	Reported in this ISR	<2% residual scatter	59
12778	MAMA Fold Distribution	0	2 [2]	1x2	Reported in this ISR	~5%	62
12779	MAMA Anomalous Recovery	0	0 [6]	contingency	N/A	N/A	66

3. Results from individual proposals

The following sections summarize the purpose, status, and results from the individual calibration proposals in the Cycle 19 program.

Proposal ID 12740: CCD Performance Monitor (PI: Svea Hernandez)

Analysis Lead, Others: Svea Hernandez

Summary of Goals and program design
This program measures the baseline performance of the CCD on STIS. It collected a series of biases and flats at different gains, in order to estimate the read noise, CCD gain, spurious charge and relative measures of charge transfer inefficiency (CTI) from the extended pixel edge response test (EPER).

Execution
Execution was nominal. The program was scheduled to execute two times during Cycle 19. Observations were taken in March 2012 and six months later in September 2012. Each execution consisted of 7 internal orbits. No changes were made to this program from the previous cycle.

Summary of Analysis and Results
The analysis was the same as for previous cycles. A more detailed description of this analysis can be found in STIS ISR 2009-02. The overall performance of the STIS CCD continued to be stable. The read noise and spurious charge remained constant throughout Cycle 19. Figure 1 shows the history of read noise values in the CCDGAIN = 1 and CCDGAIN = 4 settings measured in cycles after SM4, and Figures 2 and 3 present the spurious charge measured at CCDGAIN = 1 and CCDGAIN = 4 respectively. All of these exposures used CCDAMP = D. The extended pixel edge response (EPER) test measured the charge in the overscan bias level using flat fields. This test provided a relative measure of the CTI in the parallel and serial direction. Such measurements reflect an increase in CTI in both directions as shown in Figure 4. The CTI in the parallel direction experienced an increase of 0.3% compared to an increase of 6.6% in the serial direction. The CTI values in the serial direction continue to be one order of magnitude lower then the ones in the parallel direction.

Accuracy Achieved
Read noise error is <0.4 e- or <5% for all different gains. The error in the gain estimates is <0.08 e- or <1%. The read noise and gain errors are higher than the accuracy stated in the Phase I.

Reference Files Delivered
None.

Relevant ISRs
None.

Continuation Plans
This program has been continued in Cycle 20 as program 13130.

Supporting Details
Figure 1, 2, 3, 4 and Tables 3.

Table 3: Gain and Read Noise (RN)

Date	CCD Gain	Gain (e-/ADU)	Gain Error (e-/ADU)	RN (e-)	RN Error (e-)
March 2012	1	1.00	0.01	5.65	0.26
	2	2.04	0.03	6.82	0.15
	4	4.15	0.03	8.33	0.30
September 2012	1	1.01	0.01	5.69	0.08
	4	4.07	0.05	8.78	0.41
	8	8.10	0.08	11.7	0.26

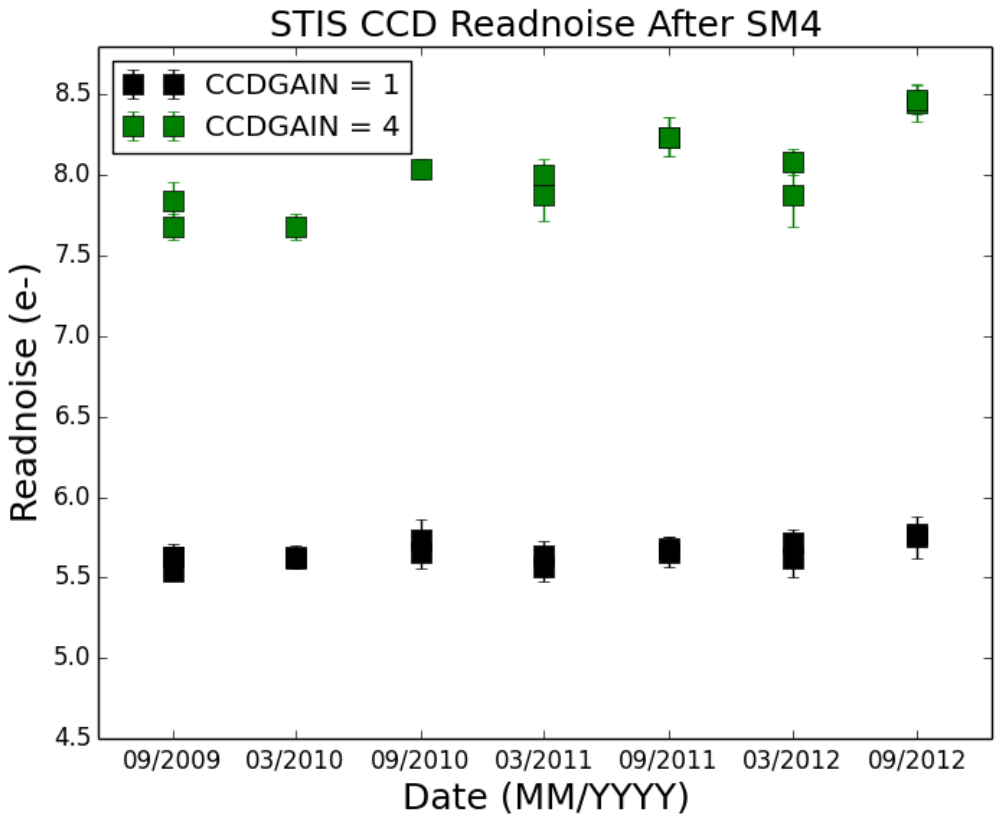

Figure 1: History of read noise after SM4 for two CCDGAIN settings using AMP D.

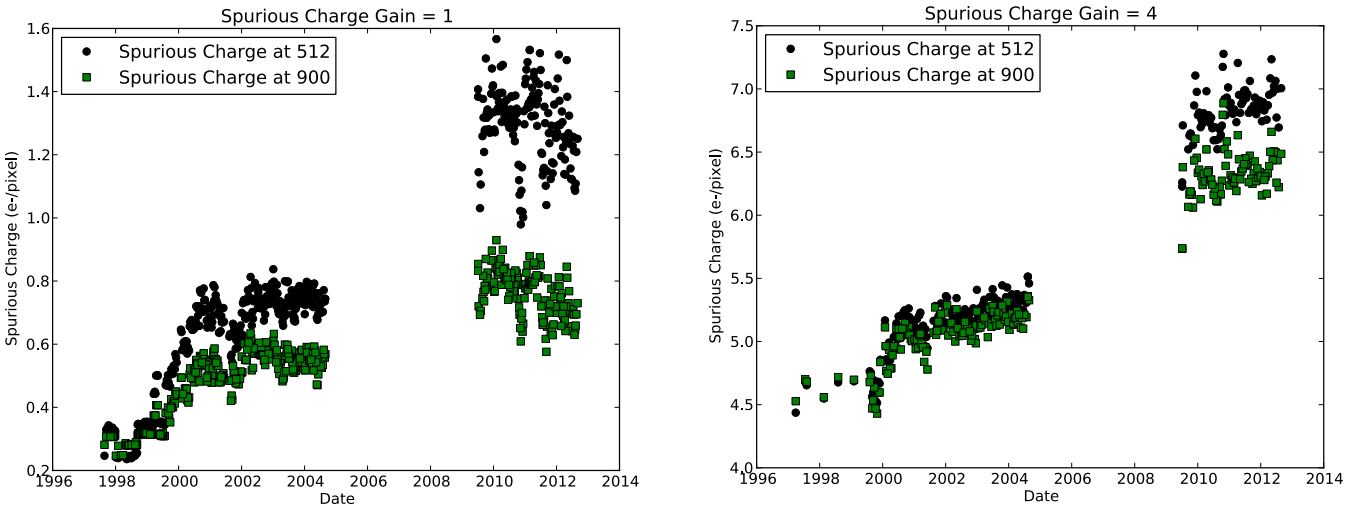

Figure 2: History of the spurious charge measured at the top and center of the CCD chip at CCDGAIN = 1 (left) and CCDGAIN=4 (right).

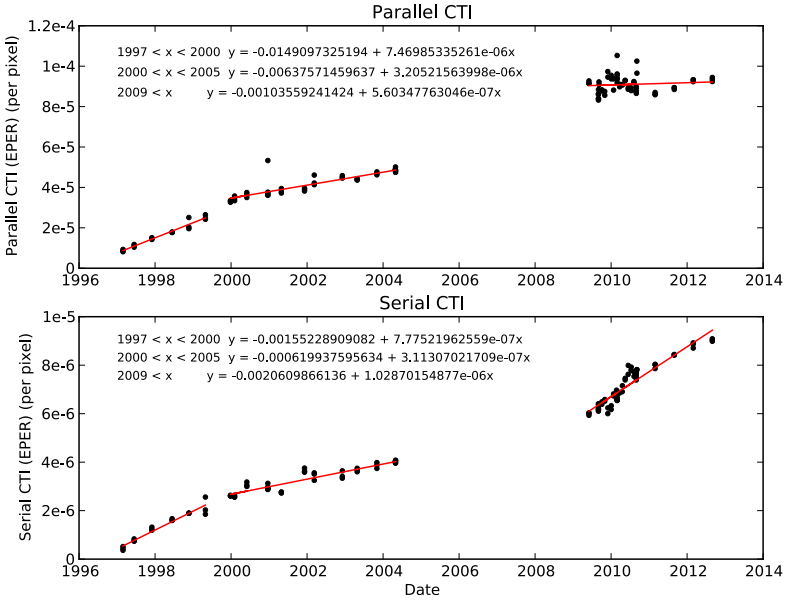

Figure 3: Top plot presents the time dependence of the measured EPER CTI in the parallel direction. Bottom plot shows the time dependence of the CTI in the serial direction. The CTI in both directions increased in the last cycle.

Proposal ID 12741 & 12742: CCD Dark Monitor Part I & II (PI: Justin Ely)

Analysis Lead, Others: Justin Ely, Svea Hernandez

Summary of Goals and program design
The program was designed to produce weekly dark reference files from a series of long dark exposures (1100s). Additionally, short dark exposures are taken daily and are available to observers for updating the hot pixel intensities in the weekly dark reference files. The program obtained darks at CCDGAIN = 1 in order to monitor the CCD behavior and chart growth of hot and bad pixels.

Execution
All 364 internal orbits were executed successfully for program 12741. Only 366 out of 368 internal orbits executed as planned in program 12742. Visits 1V and 1W lost all data in June 3, 2012 due to a SIC&DH hangup.

Summary of Analysis and Results
Darks taken between anneal periods are combined to produce a dark reference image (superdark). In the process of creating these baseline dark images, we made use of the superbiases for the corresponding time range to remove the bias from the dark reference frame. The average dark current for the period of November 2011 to October 2012 was estimated to be 0.01289 e-/s. As in previous cycles, the dark current continues to increase. The dark rate was estimated to be 0.0124 e-/s at the beginning of Cycle 19 and 0.0134 e-/s at the end of the cycle. Figure 4 presents the dark current history of the CCD as a function of time.

Accuracy Achieved
The signal-to-noise achieved on every superdark was ≈1.36, which agrees with the accuracy stated in the Phase I.

Reference Files Delivered
Approximately four superdarks were delivered each anneal period.

Relevant ISRs
None.

Continuation Plans
These two programs continued in Cycle 20 with PIDs 13131 and 13132. No significant changes have been made to the structure of the programs for Cycle 20.

Supporting Details
Figure 4.

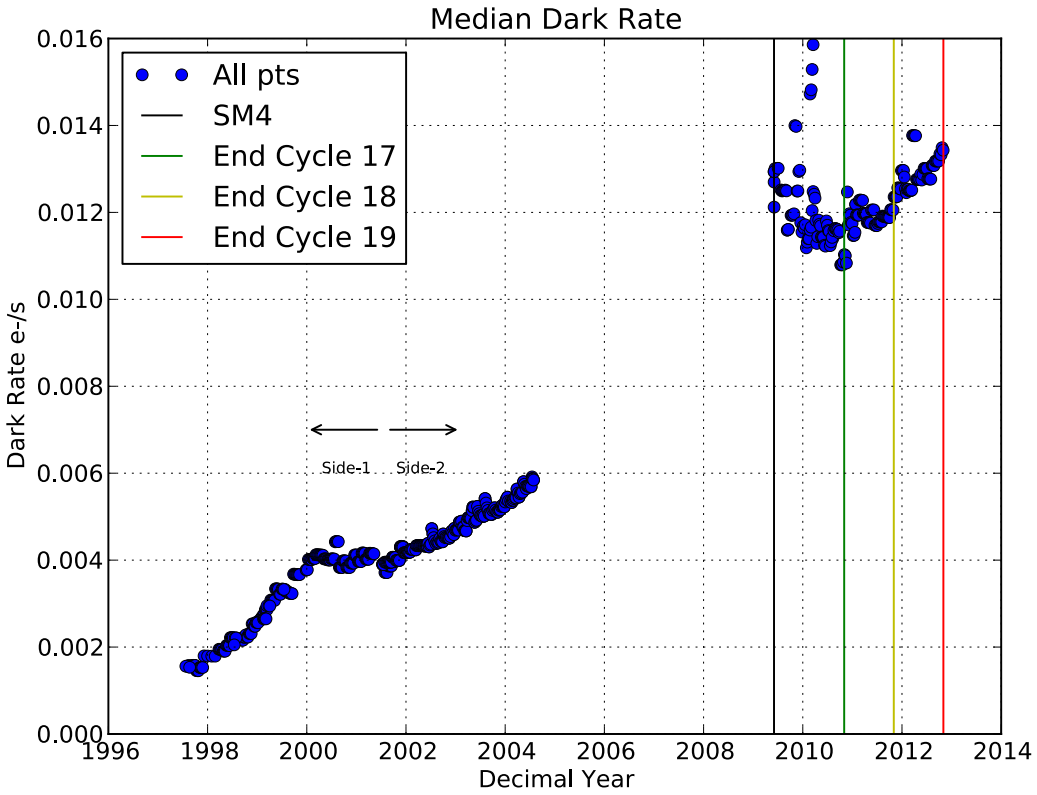

Figure 4: Dark rate vs. time. The dark rate estimates or measurements for Cycle 19 can be found between the yellow and red vertical lines.

Proposal ID 12743 & 12744: CCD Bias and Read noise Monitor Part I & II (PI: Justin Ely)

Analysis Lead, Others: Justin Ely, Svea Hernandez

Summary of Goals and program design
One of the main objectives of this program was to monitor the read noise including growth and possible fluctuations for CCDGAIN = 1 and CCDGAIN = 4 in the 1x1 bin setting read out through the nominal amplifier, D. Full frame biases were taken and read out through amplifiers A and C and used in combination with biases taken through amplifier D in order to estimate the detector's read noise. The data taken between monthly anneals was combined weekly (CCDGAIN = 1) or bi-weekly (CCDGAIN=4) to produce reference files.

Execution
Program 12743 executed 181 out of 182 of its visits successfully. Visit 0V lost all data due to an SSR3 lockup on December 1, 2011. Program 12744 executed 183 out of 184 of its visits successfully. Visit 0Y lost all data on June 3, 2012 due to a SIC&DH lockup.

Summary of Analysis and Results
Data taken between monthly anneals is combined weekly for CCDGAIN = 1 and bi-weekly for CCDGAIN = 4 to produce bias reference files. The superbiases produced have a signal-to-noise (S/N) > 1.0. The CCD read noise was estimated by measuring the RMS dispersion in a difference image previously cleaned of discordant pixels via iterative sigma clipping. These values were then plotted and compared to previous measurements in order to better monitor the read noise stability. Figure 5 presents the CCD read noise history of STIS for CCDGAIN = 1 and CCDGAIN = 4 respectively. The read noise for Cycle 19 continued to be stable with an average value of 5.73 ADUs for CCDGAIN = 1 and 2.09 ADUs for CCDGAIN = 4.

Accuracy Achieved
The program was designed to achieve a (S/N) of > 1.0 for each bias reference. Statistics on the reference files delivered are presented in Table 4. These files cover the data taken from November 2011 to August 2012. All of the products achieved a (S/N) > 1.0.

Reference Files Delivered
Approximately six superbiases were delivered each anneal period, four for CCDGAIN = 1 and two for CCDGAIN = 4.

Relevant ISRs
None.

Continuation Plans
These two programs continued in Cycle 20 with PIDs 13133 and 13151. No significant changes have been made to the structure of the programs for Cycle 20.

Supporting Details
Table 4. Figure 5.

Table 4: Bias Reference Files Delivered

CCDGAIN	Number of Files Delivered	Mean	Median	Standard Deviation	Mean S/N
1	42	1.4286	1.2053	0.9251	1.5442
4	22	2.4916	2.0686	1.8379	1.3550

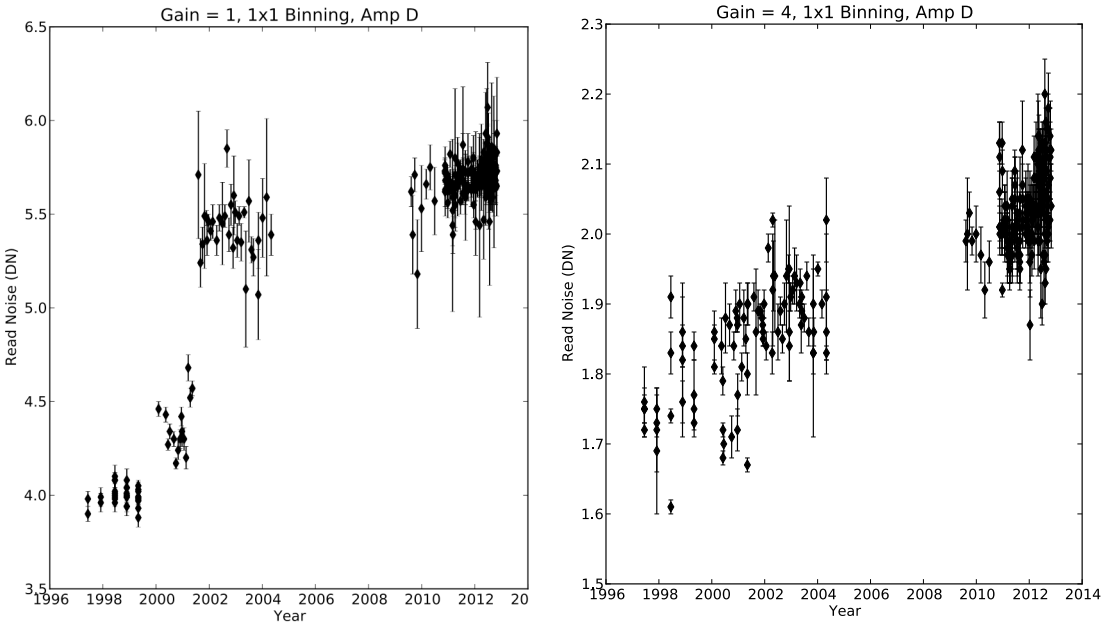

Figure 5: Read noise history for the STIS CCD at CCDGAIN = 1 (left) and 4 (right), 1x1 binning and read through amplifier D. The read noise during cycle 19 continued to be stable with an average value of 5.73 ADUs for CCDGAIN=1 and 2.09 ADUs for CCDGAIN=4.

Proposal ID 12765: CCD Hot Pixel Annealing (PI: Justin Ely)

Analysis Lead, Others: Justin Ely, Svea Hernandez

Summary of Goals and program design
The goal of this program was to anneal hot pixels and obtain statistics on hot pixels before and after the annealing. The CCD thermoelectric cooler was turned off to allow the detector temperature to rise from ~-80 C to the ambient instrument temperature of 5 C. The thermoelectric cooler was turned on 12 hours later and the CCD was cooled to its nominal operating temperature.

Execution
The program executed 1 anneal every 4th week. All 39 parallel orbits were executed successfully.

Summary of Analysis and Results
The anneal results have been posted monthly on the STIS monitors web page at http://www.stsci.edu/hst/stis/calibration/Monitors/anneal. Since the STIS CCD does not have a working temperature control circuit there is no direct measure of the CCD temperature, instead the cooling system is set to a constant current and the data is scaled to a common CCD housing temperature (keyword OCCDHTAV in the first extension [1]) before computing the monitors statistics. Even after scaling the darks to a common temperature the number of hot pixels fluctuates considerably (see figure 6) meaning that the signature of the temperature fluctuations is not removed entirely. During Cycle 19 the number of post-anneal hot pixels at level 0.1 e-/s varied between 42,556 to 55,851. It was concluded that these fluctuations in the number of hot pixels after each anneal are directly proportional to the CCD housing temperature as shown in Figure 7. Additionally, the median dark current during this cycle varied from 0.01283 counts/pixel/s to 0.01832 counts/pixel/s. Average growth rate of hot pixels is ≈9.4% per month.

Accuracy Achieved
Due to the fluctuations in the number of hot pixels after the anneals and the variations in the dark current during Cycle 19, it is difficult to derive an accurate measurement for the hot pixel growth rate.

Reference Files Delivered
No reference files are created from the anneal monitoring.

Relevant ISRs
None.

Continuation Plans
This program continued in Cycle 20 with PID 13134. No significant changes have been made to the structure of the program for Cycle 20.

Supporting Details

Figures 6 and 7.

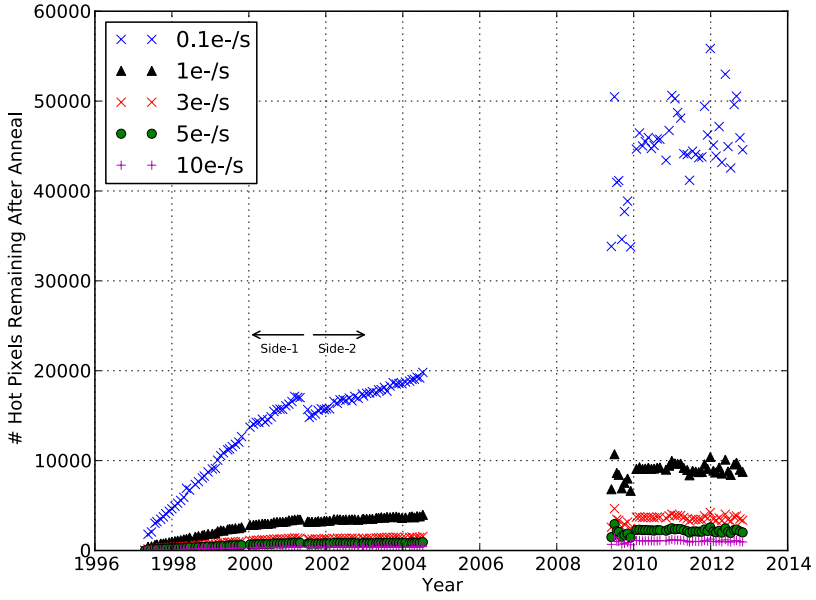

Figure 6: Number of hot pixels for various count rate thresholds remaining after a CCD anneal as a function of time. The scatter in the data is mainly caused by individual pixels being affected by accumulation of radiation damage and CCD temperature fluctuations.

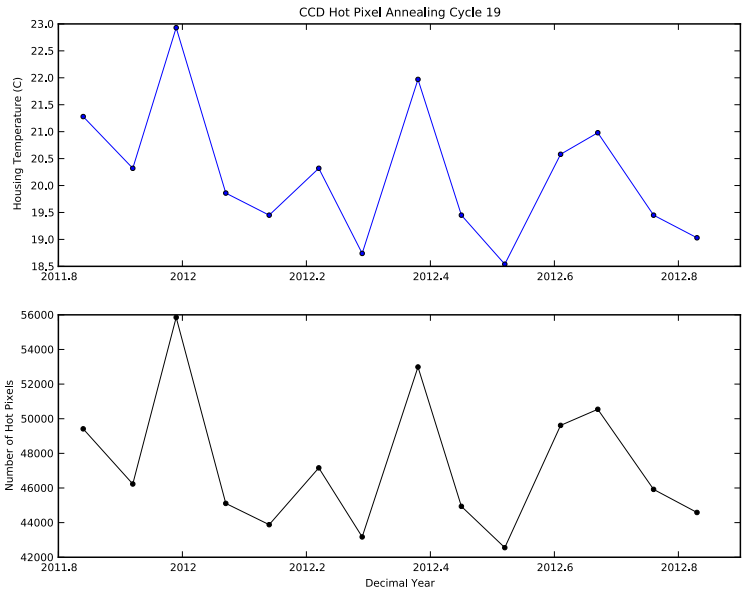

Figure 7: Top plot presents the CCD housing temperature after the anneals as a function of time. Bottom plot displays the number of hot pixels after each anneal during Cycle 19.

Proposal ID 12766: STIS CCD SPECTROSCOPIC flats (PI: Elena Mason)

Analysis Lead, Others: Elena Mason

Summary of Goals
This program aims to obtain medium resolution (MR) grating flats in order to create the p-flat for CCD spectroscopic observations (which is wavelength and virtually mode independent). The program also obtained low-resolution (LR) grating flats to monitor the low frequency variation in the LR flats, especially those induced by possible movements of the dust motes and blemishes on the CCD.

Execution
19 orbits/visits were dedicated to M grating observations. Of these, 10 orbits adopted the G430M/50CCD setup and were spread across the cycle (roughly 1 orbit every ~40 days); while, the remaining 9 orbits used the G430M/52X2 setup positioning the slit at 5 different offset positions in order to make sure that the largest area of the detector was uniformly illuminated. 18 orbit/visits were dedicated to LR grating observations. Of these, 5 orbits were used to collect flat field frames with the G430L/50CCD setup, and 10 with the G430L/52X2 setup. In the case of the latter, a setup similar to the observing strategy used for the MR grating was adopted. In addition 3 orbits were executed using the G750L/50CCD setup.

No failure of any type occurred during the execution of the program, which was completed by September 2012.

Summary of Analysis
The low resolution and the medium resolution flat exposures were processed separately and independently using an existing python code (See STIS TIR 2013-02 for more details). The code uses CALSTIS to remove bias and darks, as well as to stack (also removing cosmic rays) the frames taken across the cycle with the same setup. The products are then fit column-by-column and row-by-row in order to produce a pixel-to-pixel flat (p-flat) for each setup. These are finally combined in a reference p-flat to be used in the data reduction of Cycle 19 science observations.

Accuracy Achieved
The standard deviation of the m-mode and l-mode p-flats is 0.009850224 and 0.008665277 respectively (central 100x100 pixels of the CCD), implying an accuracy $\leq$ 1% as requested.

Reference Files Delivered
One L-mode P-flat and one M-mode P-flat have been delivered.

Relevant ISRs
“Revised version of the python code for the creation of STIS CCD P-flats” E. Mason, STIS TIR 2013-02
“STIS CCD spectroscopic P-flats” E. Mason, STIS ISR 2013-05

Continuation Plans
The program continued in Cycle 20 with only the medium-resolution grating visits. The low-resolution grating visits were dropped as the time evolution of the dust motes is expected to occur on longer time scales. Their accurate time scale evolution is being evaluated with the existing archive data and reported in STIS ISR 2013-05.

Supporting Details
N/A

Proposal ID 12767: STIS CCD IMAGING flats (PI: Elena Mason)

Analysis Lead, Others: Elena Mason

Summary of Goals
This program aims at monitoring the stability of the imaging flat field across the cycle as well as the stability from cycle to cycle. The program was a continuation of the Cycle 18 monitoring program 12406. It is identical to that with the exception of two visits which used the 50CORON aperture and which have been removed in program 12767.

Execution
Two sets of STIS CCD imaging flats were obtained 8 times during Cycle 19, within 8 visits, which were scheduled about 1.5 months apart from each other. The instrument setup used was MIRVIS/50CCD and MIRVIS/F28x50LP, standard readout from the D amplifier, and CCDGAIN = 4. No pixel binning or subarray-readouts were used. For each visit, the total integration time per instrument setup was of 1.8 s distributed across 6 exposures.

The STIS CCD imaging flat field data were collected between December 2011 and October 2012 with no failure of any kind.

Summary of Analysis
First, each flat exposure was visually inspected for any macroscopic anomalies. Second, flat frames with the same setup were processed with CALSTIS for bias and dark subtraction and combined to create one coadded, cosmic ray cleaned, super-flat per visit. These were individually analyzed and compared by taking ratios of different pairs to evaluate possible evolution over time. Finally the per-visit super-flats were combined into final cycle super-flats for each set up and compared with similar super-flats from Cycles 18 and 17.

Table 5 shows the value of the ratios and the standard deviations as measured in the central area of the detector for visits 2 through 8 super-flats after they have been divided by the visit 1 super-flat. This shows that there are no trends over time and no variations at a $\leq$ 0.32% level.

Visit Ratio	50CCD [430:640, 470:565]	F28x50LP [390:620, 460:565]
2/1	1.001847±0.002808416	1.000383± 0.003003106
3/1	0.9997543±0.002854749	1.000695±0.003048143
4/1	1.002545±0.002885342	1.001834±0.003052669
5/1	1.000767±0.003020597	1.000391±0.003207396
6/1	0.9979582±0.003016822	1.000062±0.003216082
7/1	1.003827±0.003092206	1.0004±0.003234389
8/1	0.9972944±0.003193018	0.9970782±0.003356243

Table 5. Super-flat ratios and standard deviations as measured in the central area of the detector.

Table 6 reports the average pixel value and standard deviation as measured in the central part of the detector in the ratios of the Cycle 19 super-flat, compared to the Cycle 18 and 17 super-flats. This table also shows no significant time trends; the two super-flats appear to be stable across (at least 3) cycles.

Cycle super-flat ratio	50CCD [430:640, 470:565]	F28x50LP [390:620, 460:565]
19/18	0.995665 ± 0.001891802	0.9636449 ±0.002246395
19/17	0.9956784 ± 0.001925304	0.9976374 ± 0.001697015

Table 6. Average pixel value and standard deviation as measured in the central part of the detector

Accuracy Achieved
We achieved an average count level per pixel (measured in the central detector area, free from defects and dust motes) of 78341 ADU per visit for the 50CCD "visit super-flats" and 64263 ADU per visit for the F28X50LP super-flats. The average standard deviation is ~677 and 547 ADU, respectively. This converts to a percent Poisson noise of 0.36 % and 0.39%, per visit, for the 50CCD and F28x50LP super-flats, respectively; and to an intrinsic noise of 0.79% and 0.75% per visit for the 50CCD and F28X50LP super-flats, respectively, again.

When the Cycle 19 super-flats are considered the average count level per pixel is 626631 and 514112 ADU in the 50CCD and F28x50LP super-flat, respectively. The expected Poisson and actual intrinsic noise are 0.13% and 0.84% for the 50CCD, and 0.13% and 0.81% for the F28X50LP super-flat.

Reference Files Delivered
N/A

Continuation Plans
The program was substantially revised in Cycle 20. The number of visits has been halved in Cycle 20 and the monitoring of the long pass filter F28x50LP has been dropped. In addition, each of the 4 visits foreseen for Cycle 20 will contain one short exposure with the 50CORON aperture to 1) test the reproducibility of such aperture and 2) evaluate the possible need for a 50CORON L-flat for the reduction of 50CORON science data.

Supporting Details
Table 5 and 6.

Proposal ID 12768: CCD Spectroscopic Dispersion Solution Monitor (PI: Paule Sonnentrucker):

Analysis Lead, Others: Paule Sonnentrucker

Summary of Goals:
Constrain STIS CCD dispersion solution using internal HITM1 wavecal data for all 6 gratings supported for CCD spectroscopic observations. There were no external targets used.

Execution:
Yearly program executed on Oct 17, 2011 using a total of 3 visits of 1 internal orbit each. The data using the G230LB, G230MB, G430L, G430M, G750L and G750M gratings were all successfully taken. The 52X0.1" slit was used in all cases. No data loss occurred.

Summary of Analysis:
The HITM1 lamp exposures were reduced with CalSTIS as if they were science exposures. The emission lines in the resulting x1d spectra were compared to the laboratory wavelengths. The comparison between the lamp lines and the laboratory lines was done using three different methods:

1. Spk Method: Compute difference (in pixels) between the laboratory line and the peak of the emission in a range corresponding to 0.5 pixels from expected centroid.
2. Gaussian Method: Fit a Gaussian to each emission line in the spectrum and compute difference between the laboratory line and the Gaussian centroid.
3. WeightSpk Method: Compute the emission line centroid weighted mean by using the counts over 2 pixels on each side of the line centroid as weights.

For each mode the mean and standard deviation of the latter differences were then calculated.

Accuracy Achieved:
The mean of the difference distribution is lower or equal to 0.1 pixel and the standard deviation is lower than 0.35 pixel in all cases. 1 pixel corresponds to 175 km/s for G230LB and 20 km/s at 2300 Å for G230MB. These results are consistent with those reported for Cycle 17 by Pascucci et al. (STIS ISR 2010-01) and Cycle 18.

Reference Files Delivered:
No new files have been delivered yet, as the solution accuracy has not changed since Cycle 17.

Relevant ISRs:
These results along with all accompanying figures will be included in a multi-cycle ISR (Sonnentrucker P. 2015, in prep).

Continuation Plans:
Monitoring program for the CCD dispersion solution was carried over to Cycle 20 with Program 13137 for a total of 3 orbits, 1 visit each, as in Cy19.

Supporting Details:
Below are, in form of a series of tables and representative figures, the summary of the mean and standard deviations for each grating/cenwave combination derived from the monitoring data analysis.

Table 7: Accuracy achieved for the G230LB and G230MB gratings

Grating-Cenwave	Mean Offset (pix)	Standard Dev (pix)
G230LB- 2375	0.03	0.32
G230MB- 1713	0.07	0.32
- 1995	0.02	0.27
- 2416	0.01	0.22
- 2697	-0.05	0.20
- 3115	-0.02	0.21

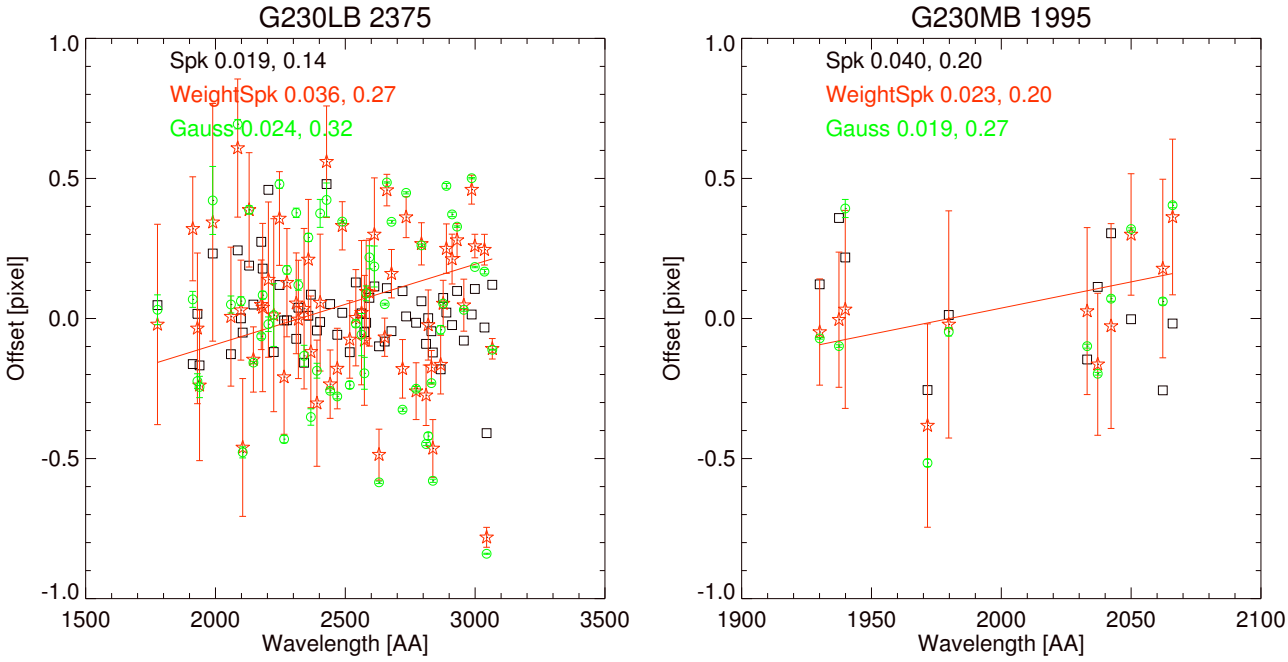

Figure 8: Difference between fitted line centroids and corresponding laboratory wavelengths for all identified lamp lines for the G230LB (left) and G230MB (right). The line represents a linear fit to the difference obtained through the WeightSpk method. The two values listed for each method represent the mean offset and standard deviation respectively.

Table 8: Accuracy achieved for the G430L and G430M gratings

Grating-Cenwave	Mean Offset (pix)	Standard Dev (pix)
G430L- 4300	0.04	0.26
G430M- 3165	0.10	0.11
- 3680	-0.03	0.33
- 4961	-0.10	0.11
- 5471	0.04	0.08

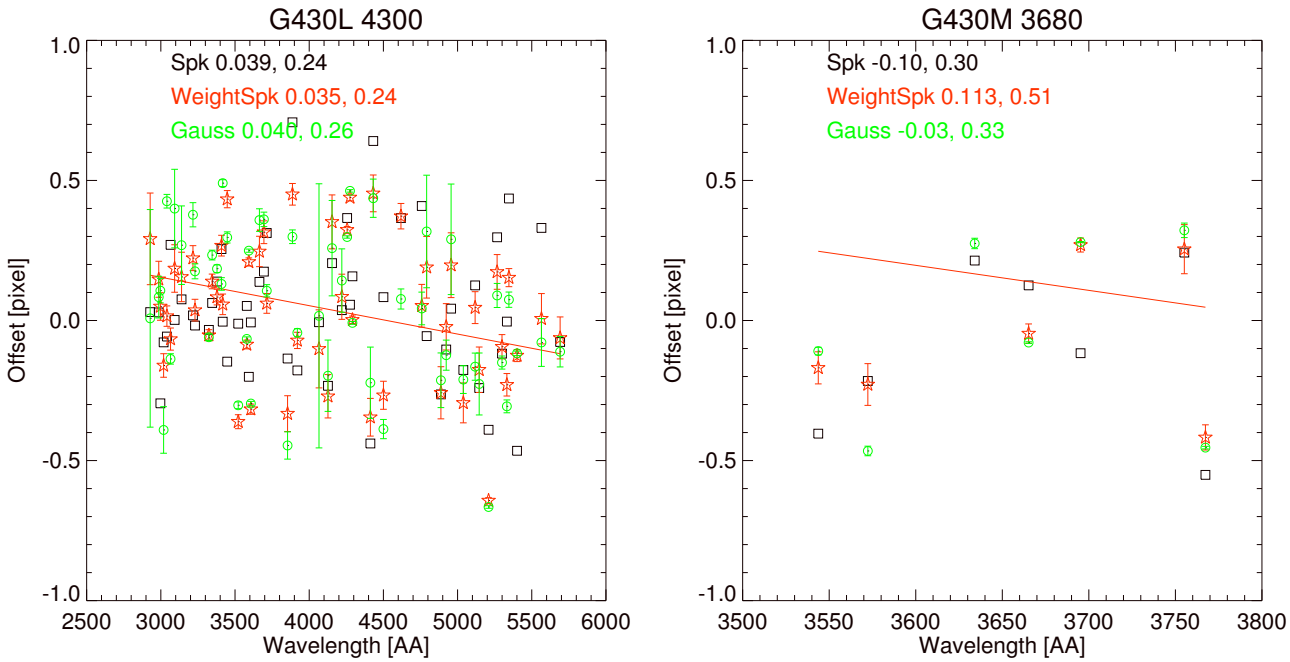

Figure 9: Difference between fitted line centroids and corresponding laboratory wavelengths for all identified lamp lines for the G430L (left) and G430M (right). The line represents a linear fit to the difference obtained through the WeightSpk method. The two values listed for each method represent the mean offset and standard deviation respectively.

Table 9: Accuracy achieved for the G750L and G750M gratings

Grating-Cenwave	Mean Offset (pix)	Standard Dev (pix)
G750L- 7751	-0.10	0.14
G750M- 5734	-0.03	0.08
- 6768	-0.02	0.04
- 8311	0.00	0.07
- 9336	-0.03	0.08

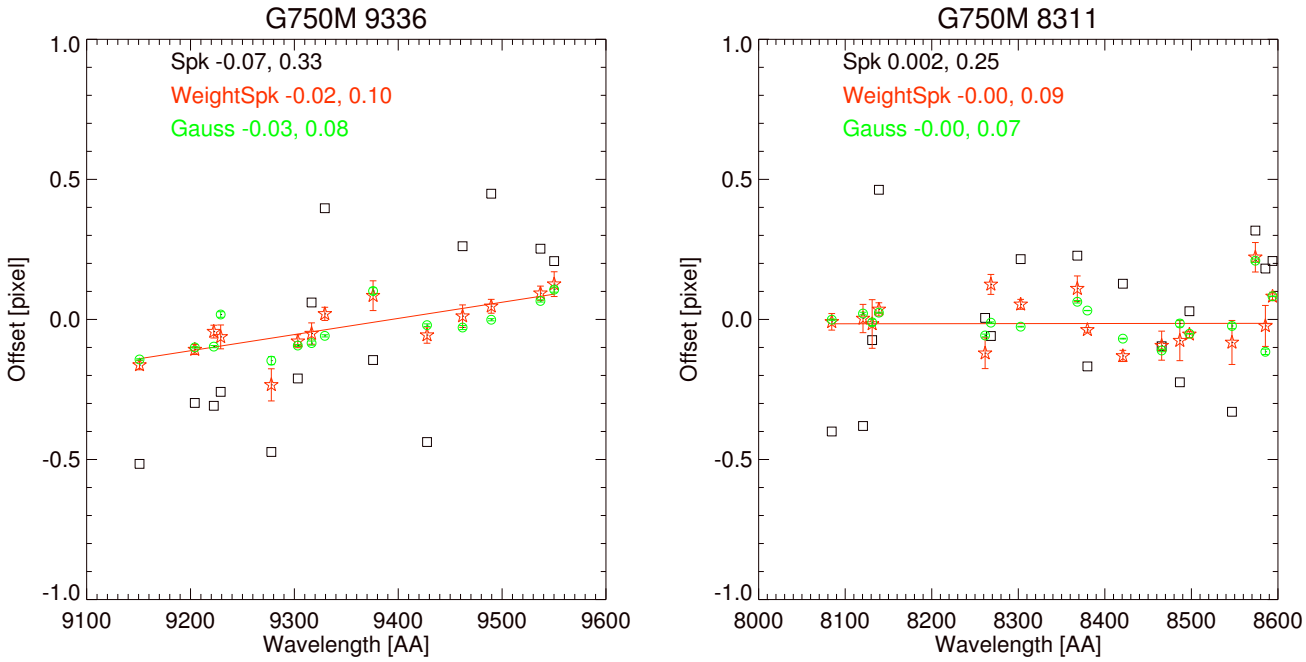

Figure 10: Difference between fitted line centroids and corresponding laboratory wavelengths for all identified lamp lines for the G750L (left) and G750M (right). The line represents a linear fit to the difference obtained through the WeightSpk method. The two values listed for each method represent the mean offset and standard deviation respectively.

Proposal ID 12769: CCD Sparse Field CTE (PI: Michael Wolfe)

Analysis Lead, Others: Michael Wolfe, Svea Hernandez

Summary of Goals and program design
The purpose of this program is to establish an accurate correction for parallel register CTE losses. Additionally, the program tests the effects of different bias voltages by executing its observations both at GAIN=1 and GAIN=4. Final values for the CTE correction coefficients are used to update the CCDTAB reference file when needed.

Execution
The program was scheduled to execute in two different periods during Cycle 19. The first part of the program was scheduled for November 2010 and the second part for December 2010. Most visits executed nominally with the exception of visits 62, 63, 64, 75, 76 and 77. Minutes before visit 62 executed the data recorder unexpectedly stopped. All six visits executed nominally but the data was not recorded. These failed visits were replaced by F2, F3, F4, G5, G6 and G7 respectively.

Summary of Analysis and Results
Internal calibration lamp observations were taken with narrow slits and used in measuring the sparse field CTE. Slit images are projected at five different positions on the detector. Multiple exposures are taken at each position alternating between amplifiers A and C for readout. For each exposure, the average flux per column and centroid of the image profile within a standard 7-row extraction box are estimated. The observed ratio of the fluxes seen by the two amplifiers is fit to a simple model of constant fractional charge loss per pixel transfer. The CTI values are considered to be the fits to the observed flux ratio at a range of source positions along the columns. As in previous cycles it has been concluded that the centroid shifts are directly proportional to the CTI.

Accuracy Achieved
CTI values are accurate to within 1% for signal levels > 200 e-.

Reference Files Delivered
None.

Relevant ISRs
None.

Continuation Plans
This program has been continued in Cycle 20 as program 13138.

Supporting Details
See Figures 11 and 12.

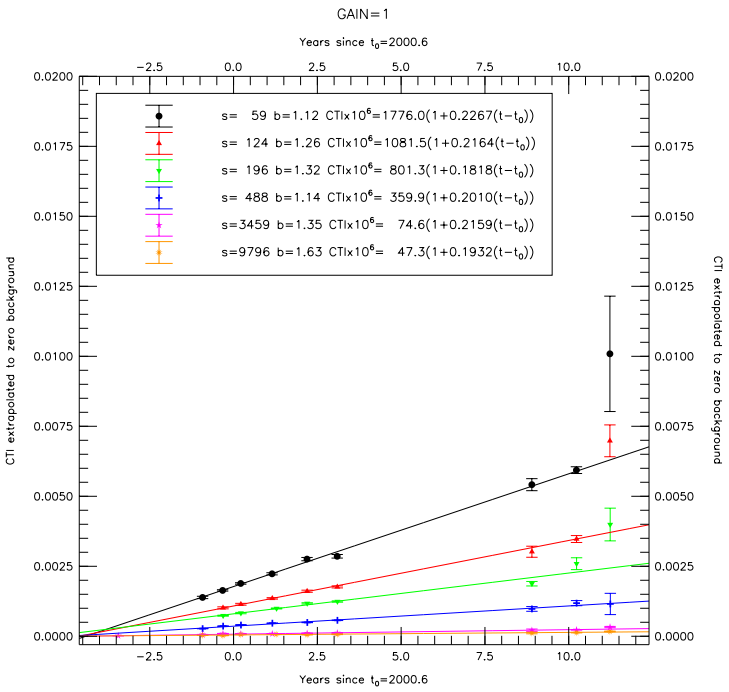

Figure 11. CTI for GAIN=1 as a function of Time. The values are identified for a specific source (s) and background (b)

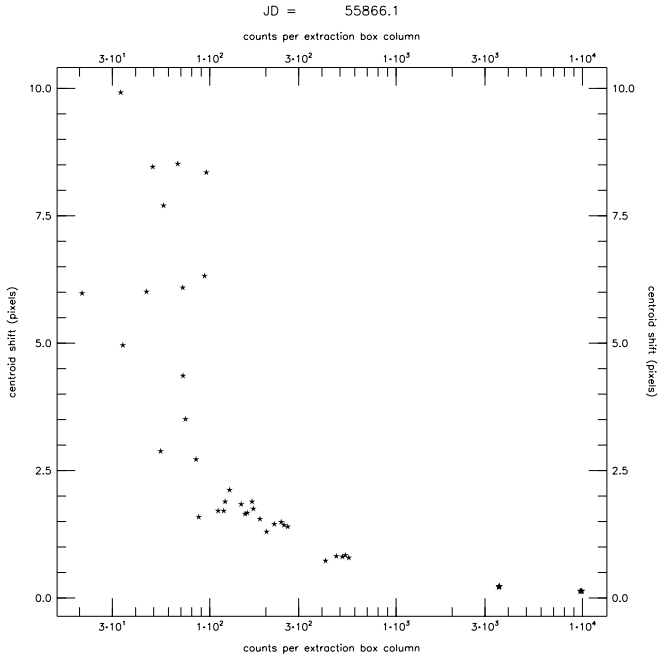

Figure 12. Centroid shift for the central location on the CCD as a function of signal level

Proposal ID 12770: STIS CCD Full-Field Sensitivity Monitor (PI: Julia Roman-Duval)

Analysis Lead, Others: Julia Roman-Duval

Summary of Goals: Measure a photometric standard star field in Omega Cen (NGC5139) in 50CCD annually to monitor CCD sensitivity over the whole field of view. This test gives a direct transformation of the 50CCD magnitudes to the Johnson-Cousins system for red sources. These transformations should be accurate to 1%. The stability of these transformations is measured to the sub-percent level. These observations also provide a check of the astrometric and PSF stability of the instrument over its full field of view.

Execution
Execution occurred as planned between 02-09-2012 3:05 and 2-10-2012 01:08.

Summary of Analysis
The sensitivity of the STIS CCD is observed to decrease linearly with time, with a rate measured from the STIS sensitivity monitors. The TDS trends are thus obtained from spectroscopic observations, and implemented in CALSTIS for both imaging and spectroscopic STIS CCD observations. The goal of the full-field sensitivity analysis is to verify that the TDS trends derived from spectroscopic observations are applicable to imaging mode.

The star field NGC5139 is observed annually with the 50CCD (clear) filter as part of the STIS full-field sensitivity calibration program. Calibrated and geometrically corrected science files (*sx2.fits) for all STIS CCD full-field sensitivity programs up to C19 were retrieved from MAST. The data set used in this analysis thus includes programs acquired since 2000 up to 2012 (program IDs: 8847, 8912, 9622, 10028, 11854, 12409, 12770).

All exposures, obtained with different guide stars, show astrometric offsets of ~1". We first register all exposures with the following method. A reference exposure is chosen, taken as part of program 11854 (obat01050_sx2). The cross-correlation function of the reference exposure and each exposure of the data set is calculated using the IDL routine CORREL_IMAGES, and its maximum located using the IDL routine CORRMAT_ANALYZE. The location of the maximum of the cross-correlation function corresponds to the shift to be applied to the image to match its astrometry to the reference exposure.

Once all exposures are astrometrically registered to the reference exposure, a catalog of stars is identified in the reference exposure using starfinder. The input parameters of starfinder, such as minimum correlation and detection threshold, were empirically determined via a trial-and-error method. We chose a detection threshold of 10 σ and a minimum correlation of 0.7. Pairs of stars closer than 0.8" were excluded from the catalog. The starfinder point source extraction algorithm requires a PSF to match the shape of point sources to. We derived the PSF directly in each image using a pre-

determined list of stars identified by eye. Each star is centroided and stacked with the IDL routine PSF_EXTRACT in order to estimate the PSF.

Our algorithm then performs aperture photometry for each star in the catalog and each STIS CCD exposure. First, the background, its standard deviation, and the FWHM of the PSF are estimated in each exposure. Second, an accurate position for each star in the catalog in each exposure is determined. Our registration algorithm is accurate to 1 pixel. Therefore, a test sub-image centered on the position of a star from the catalog, and of width 0.8" is first used to estimate the centroid position of each star in each exposure with sub-pixel accuracy. Once the centroid position is determined, a second sub-image is extracted of size 0.8" and centered on the previously calculated centroid position. Aperture photometry is performed on this sub-image, using an aperture of 5 times the FWHM of the PSF, and annulus also of radius 5 times the FWHM of the PSF, and thickness 5 pixels. The net counts are then converted to magnitudes using the exposure time and the ZMAG keyword populated by CALSTIS, and which includes a correction for the expected TDS trend.

Our algorithm thus provides a catalog of stars and their magnitudes as a function of time, covering the time period 2000-2012. For each star, a linear trend magnitude vs time is fitted (see Figure 13). Figure 14 shows the histogram of the slopes of these trends. The mean weighted slope of the magnitude vs time trend for the STIS CCD detector is 0.5 mmag/year, with a standard deviation of 16 mmag/year (based on 106 stars). Over 16 years, this represents a change of 0.6%, lower than the quoted 1 % uncertainty. Figure 15 shows the time dependency of the full-field sensitivity (expressed as a slope in mmag/year) as a function of magnitude.

Accuracy Achieved
<1%

Reference Files Delivered
None

Relevant ISRs
STIS ISR 2013-02 (Roman-Duval et al. 2013)

Continuation Plans
Continued in Cycle 20 as program 13139.

Supporting Details

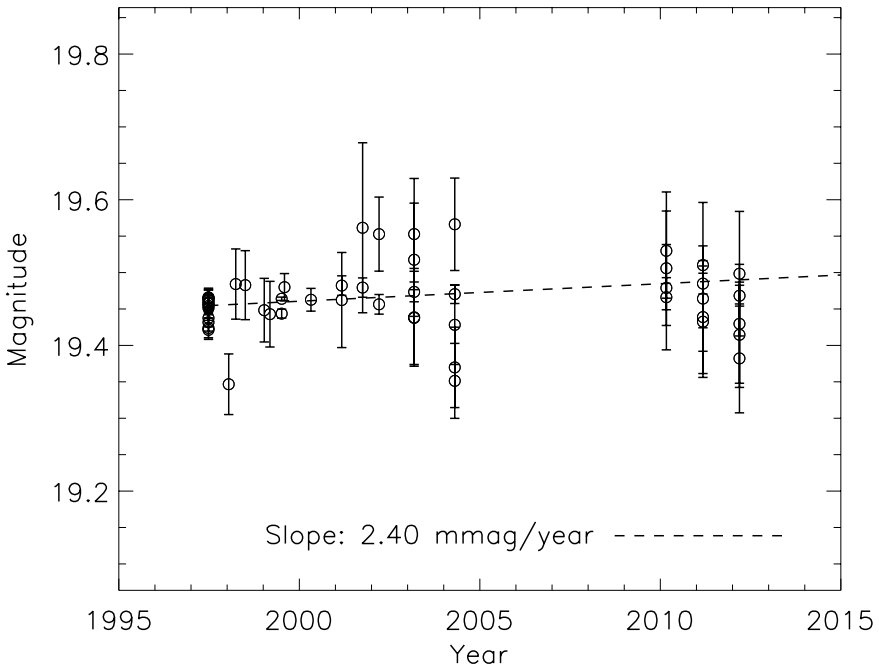

Figure 13: Example of time-dependent full-field sensitivity analysis for a star from the CCD star catalog.

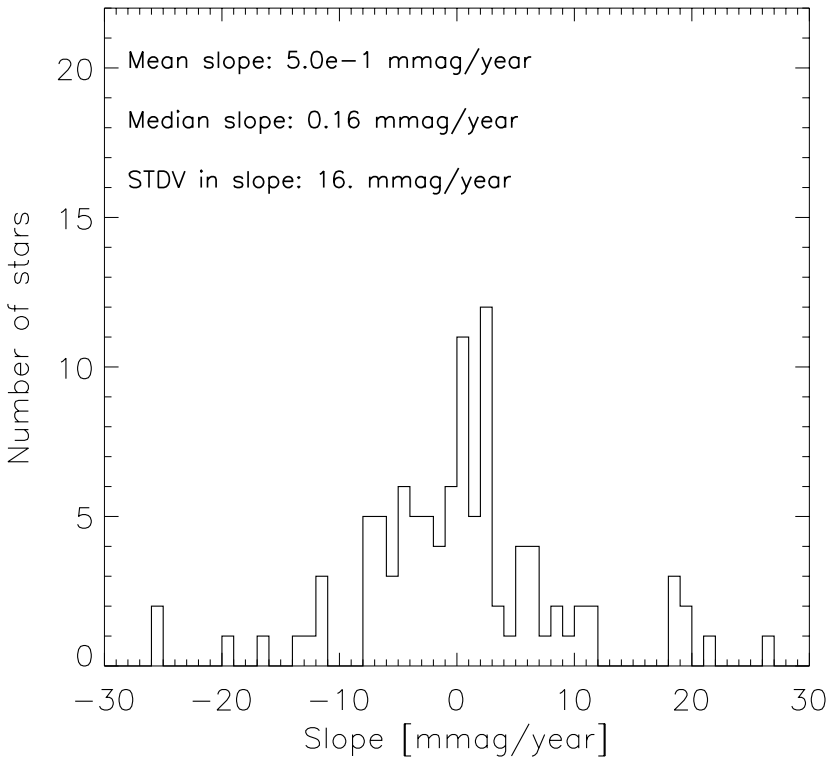

Figure 14: Histrogram of the time dependency of the full-field sensitivity for the STIS CCD.

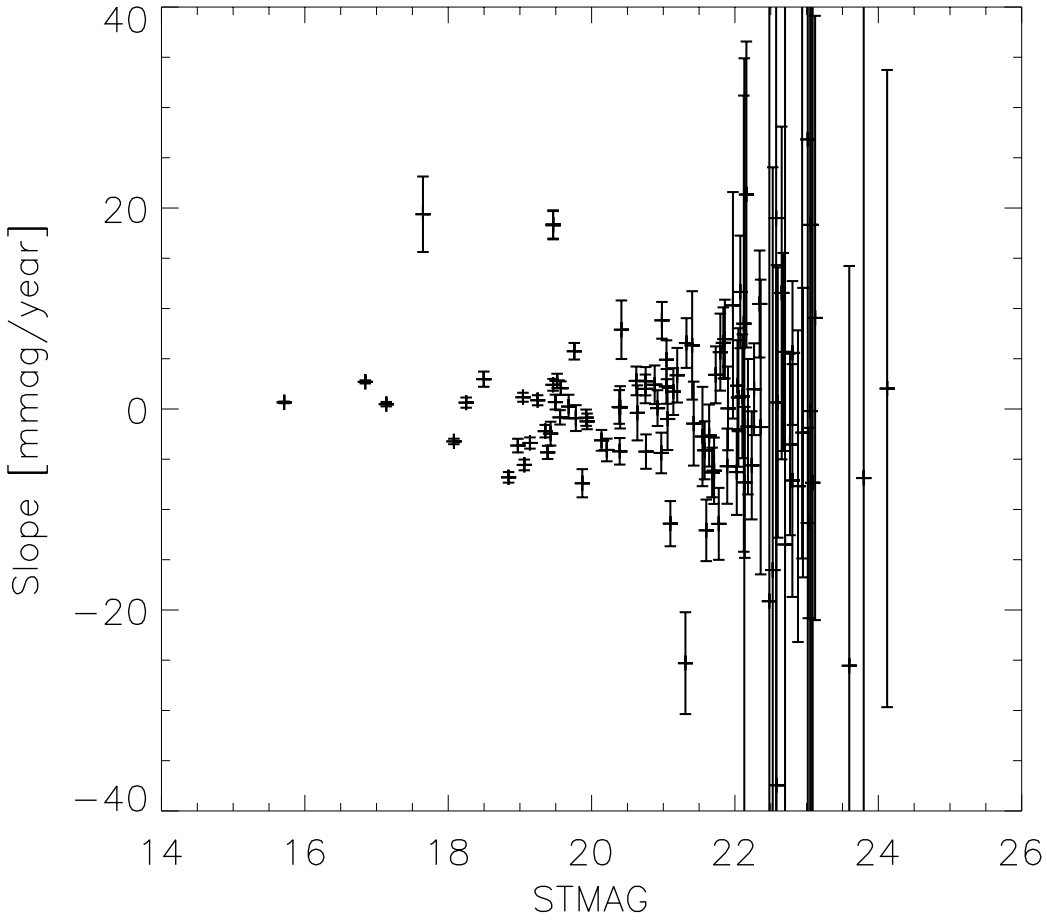

Figure 15: Residual flux calibration error on the imaging mode as a function of magnitude in the STIS CCD detector.

Proposal ID 12771: Slit Wheel Repeatability (PI: Chris Long)

Analysis Lead: Audrey DiFelice

Execution:
Executed nominally on December 2, 2011

Summary of goals;
Check the repeatability of the STIS slit wheel motion from a sequence of lamp spectra using the grating G230MB (centered at 2697 Å) and the three smallest long slits (52X0.1, 52X0.2, and 52X0.05).

Summary of analysis
A total of 24 exposures were taken over the course of approximately 40 minutes. 9 exposures were taken with the 52X0.1 slit, 8 exposures were taken with the 52X0.2 slit, and 7 exposures were taken with the 52X0.05 slit. The data were processed with the WAVECAL function. The Cycle 19 SHIFTA1 data (the shift in the dispersion direction) seemed to follow the trends of previous cycles. The SHIFTA2 data (the shift in the spatial direction) has not trended strongly over previous cycles, but the Cycle 19 data lies within the bounds of previous cycles. The first data point in each of the three sets was used as a reference point, and all subsequent measurements were zeroed to that reference. The thermal effects of the motion of the slit wheel were then modeled as second order polynomials and subtracted out. After these corrections were applied, the resulting average absolute shift in the dispersion direction (SHIFTA1) was found to be 0.009 pixels, and the resulting average absolute shift in the spatial direction (SHIFTA2) was found to be 0.013 pixels

Accuracy achieved:
The slit wheel is repeatable to an accuracy of 0.013 pixels

Continuation plans:
Continued in Cycle 20 as Program 13140

Proposal ID 12772: STIS/CCD Spectroscopic Sensitivity Monitor for Cycle 19 (PI: Azalee K. Bostroem)

Analysis Lead, Others: Stephen Holland**,** Azalee Bostroem

Summary of Goals and program design
The purpose of Program 12772 is to monitor the spectroscopic sensitivity of the STIS CCD. This was done using the low resolution gratings. We observed the white dwarf AGK+81D266 with the instrument configurations listed in Table 10. The datasets from these observations are also listed in Table 10. Datasets in italics had some problem that led us to ignore them when computing the TDS parameters.

We took the ratio of the flux in each spectrum to the flux in a reference spectrum from early in the STIS mission and used these ratios to determine how the STIS CCD sensitivity has changed over time for each spectral element. No ratios were computed in the cases indicated by a reference spectrum of N/A.

There were no changes to this program from Cycle 18.

Execution
Observations were taken between once and four times during the program depending on the mode. The number of observations for each mode is listed in Table 10. There were no missed visits and no observatory or pipeline problems with the data from any of the four visits.

Summary of Analysis and Results
The STIS time-dependent sensitivity (TDS) software has been rewritten. This new TDS software was used to analyze this data. The major changes to the software are

- all IDL code has been rewritten in python,
- the number and times of the break points are determined automatically using an F test,
- an error that caused the CTE correction to be applied incorrectly was fixed,
- an error in the way that the dark current was computed has been corrected,
- an error that allowed ratios of mis-matched echelle orders was fixed, and
- several consistency checks have been added to ensure that ratios are computed only for data with the same instrument configuration.

The TDS software works by taking the ratio of the flux in each spectrum to the flux in a reference spectrum from early in the STIS mission. A segmented line is fit to these ratios to determine how the STIS MAMA sensitivity has changed over time for each spectral element. The fitting is blind and does not allow for discontinuities in the TDS.

There is no evidence for any change in the TDS trends during Cycle 19 for any of the modes analyzed for Program 12772. The results for the L modes are presented in Figures

16, 17, and 18, and in Tables, 11, 12, and 13. The TDS for the M modes behaves similarly to the corresponding L modes.

Much of the data for G430M/4194 prior to Program 12272 were taken with GAIN = 4 whereas the reference spectrum had GAIN = 1. We did not fit TDS slopes to these data.

Accuracy Achieved
Table 14 gives the root mean square (RMS) values for the best-fit slopes to the TDS for each mode. There was no fit to the G430M/4194 data because the data was taken with two different gain settings.

Reference Files Delivered
The following synphot reference files for STIS make use of 12772 data and only list the latest delivered versions. The files below were delivered on Apr 13, 2012.

- stis_ng31_010_syn.fits – CCD/G430L
- stis_ng32_010_syn.fits – CCD/G430L
- stis_ng41_010_syn.fits – CCD/G750L
- stis_ng42_010_syn.fits – CCD/G750M
- stis_ng21b_009_syn.fits – CCD/G230LB
- stis_ng22b_009_syn.fits – CCD/G230MB
- stis_nm36_013_syn.fits – CCD/MIRVIS

Relevant ISRs
No ISRs have been published using data from Program 12772.

Continuation Plans
This program is continued in Cycle 20 as 13141. There are no changes from program 12772.

Supporting Details

Table 10: Observations and datasets for Program 12772

Spectral Element	Aperture	Wavelength (Å)	Number (visits)	Datasets	Reference Spectrum
G230LB	52X2	2375	3	obvnl1020 obvnl2020 obvnl3020	o45a01010
G230LB	52X2E1	2375	3	obvnl1010 obvnl2010 obvnl3010	N/A
G430L	52X2	4300	4	obvnl1030 obvnl2030 obvnl3030	o45a01020

				obvnm1090 *obvnm10a0* obvnm10b0 *obvnm10c0* *obvnm10d0* *obvnm10f0*	
G430L	52X2E1	4300	4	obvnl1040 obvnl2040 obvnl3040 obvnm10e0	N/A
G750L	52X2	7751	3	obvnl1060 obvnl2060 obvnl3060	o45a01030
G750L	52X2E1	7751	3	obvnl1050 obvnl2050 obvnl3050	N/A
CCDFLAT	0.3X0.09	7751	3	obvnl1070 obvnl2070 obvnl3070	N/A
CCDFLAT	52X0.1	7751	3	obvnl1080 obvnl2080 obvnl3080	N/A
G230MB	52X2	1995	1	obmzm1010	o45a02010
G230MB	52X2E1	1995	1	obmzm1020	N/A
G230MB	52X2	2416	1	obmzm1030	o45a02020
G230MB	52X2E1	2416	1	obmzm1040	N/A
G430M	52X2	3165	1	obvnm1050	o45a02030
G430M	52X2E1	3165	1	obvnm1060	N/A
G430M	52X2	4194	1	obvnm1080	o45a02040
G430M	52X2E1	4194	1	obvnm1070	N/A
G750M	52X2	7283	1	obvnm10g0	o45a02050
G750M	52X2E1	7283	1	obvnm10h0	N/A
CCDFLAT	0.3X0.09	7283	1	obvnm10i0	N/A
CCDFLAT	52X0.1	7283	1	obvnm10j0	N/A

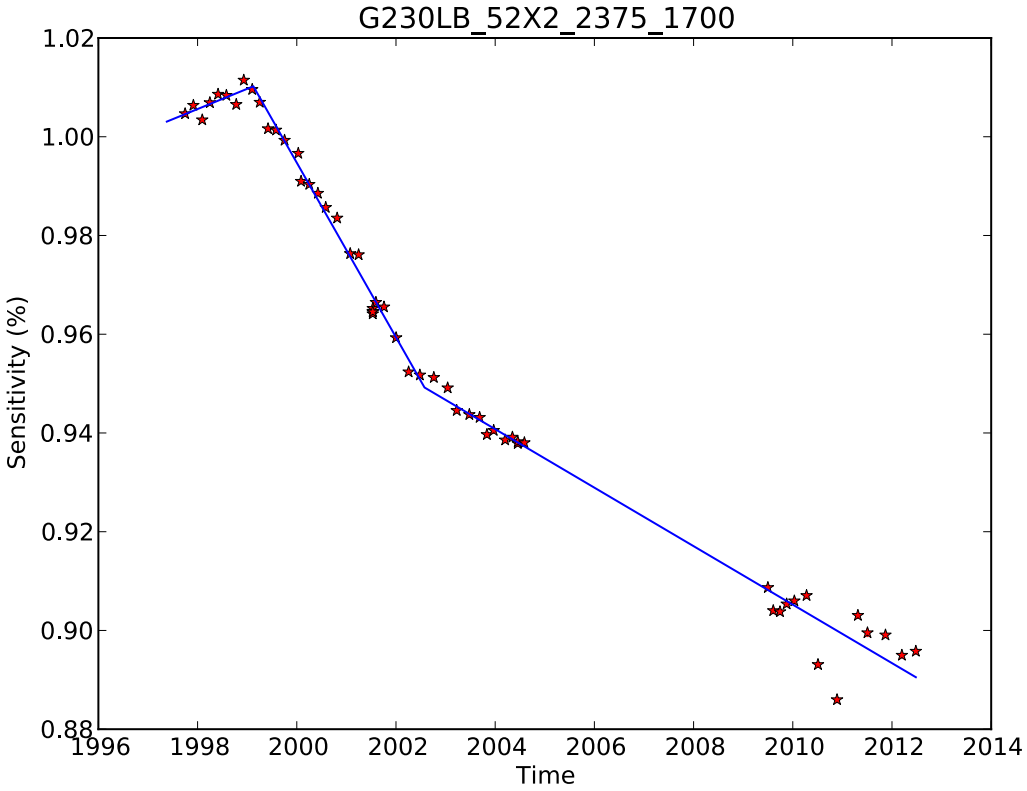

Figure 16: STIS G230LB Time-Dependent Sensitivity. The final three data points are from Program 12772. These points show no indication of a change in the TDS decay. The source of the large amount of scatter in the data since 2009 is under investigation.

Table 11: STIS G230LB Time-Dependent Sensitivity Parameters

Breakpoint	**Slope (%/year)**	**Intercept**
	+0.40966 ± 0.17573	1.00307 ± 0.00192
1999.12 ± 0.09	–1.76794 ± 0.06096	1.04106 ± 0.00421
2002.58 ± 0.15	-0.59239 ± 0.02087	0.97999 ± 0.00566

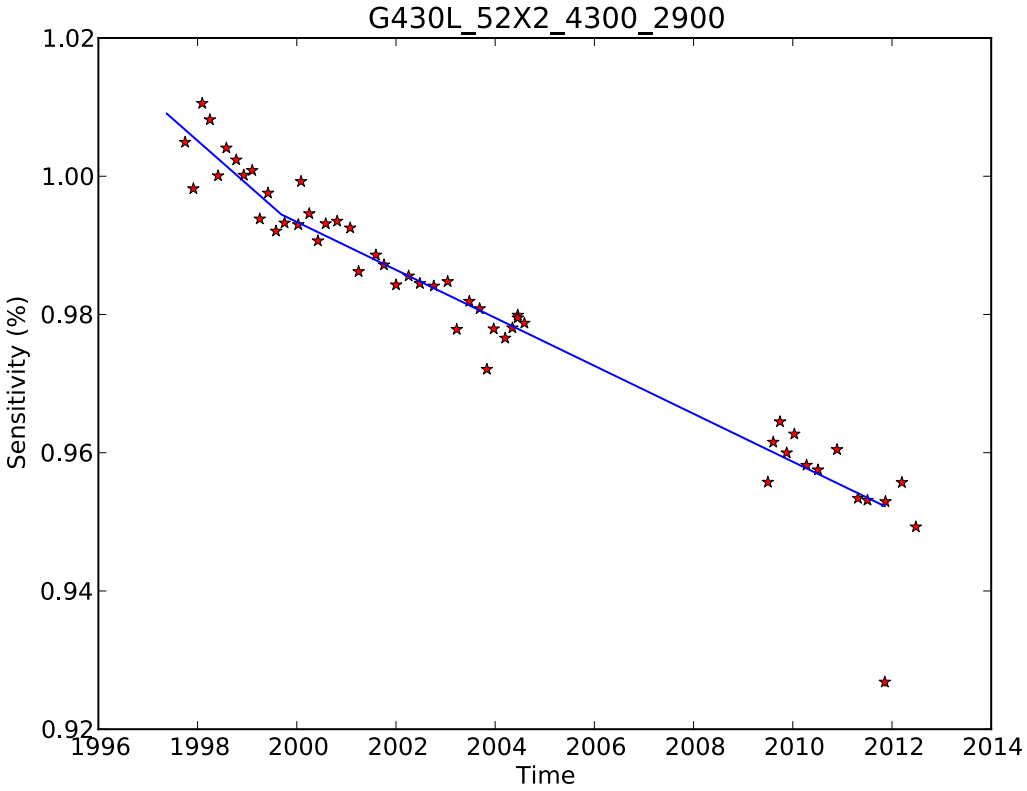

Figure 17: STIS G430L Time-Dependent Sensitivity. The final four data points are from Program 12772. Three of these points show no indication of a change in the TDS decay. The point with a sensitivity of 0.927 (obvnm10b0) is under investigation. Datasets obvnm1090, obvnm10a0, obvnm10c0, obvnm10d0, and obvnm10f0, were taken with non-zero values for POSTARG2, and are not shown in this Figure. All of the data in this Figure has POSTARG2 = 0.

Table 12: STIS G430L Time-Dependent Sensitivity Parameters

Breakpoint	**Slope (%/year)**	**Intercept**
	–0.63165 ± 0.17159	1.00905 ± 0.00242
1999.69 ± 0.78	–0.34695 ± 0.01450	1.00248 ± 0.00516

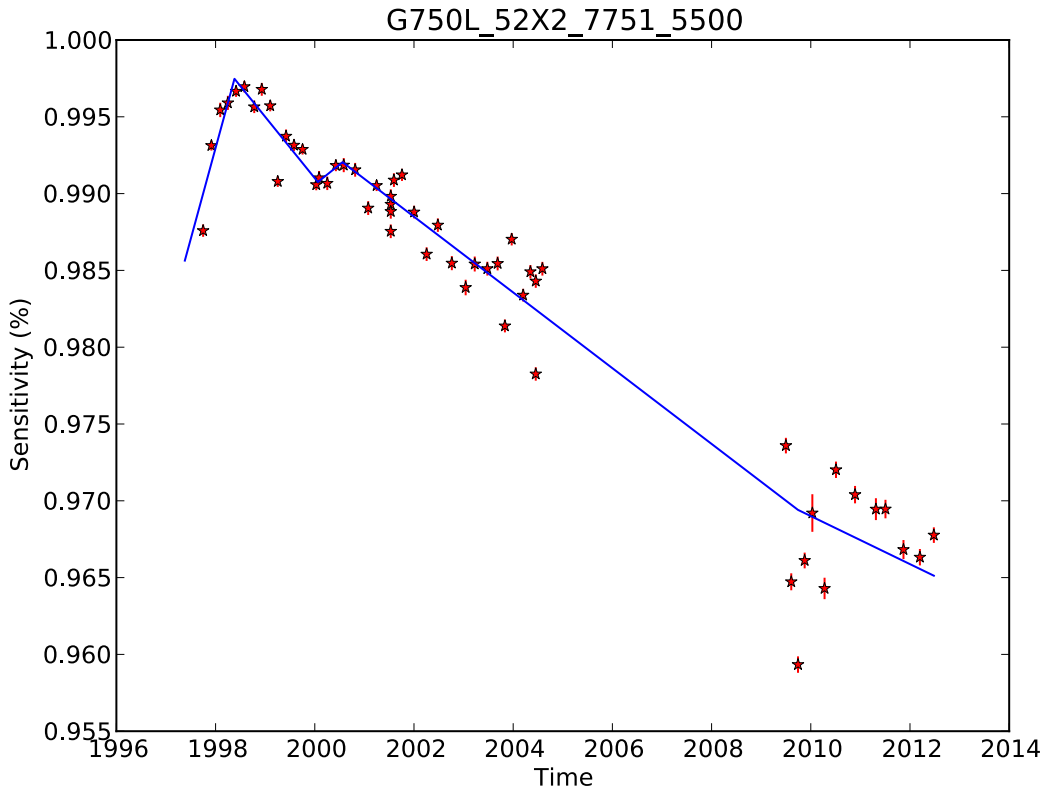

Figure 18: STIS G750L Time-Dependent Sensitivity. The final six data points are from Program 12772. These points show no indication of a change in the TDS decay. The points in late 2009 and early 2010 that have low sensitivities are under investigation. The G750L TDS data shown an unusual amount of scatter, so the fit should be treated with caution.

Table 13: STIS G750L Time-Dependent Sensitivity Parameters

Breakpoint	**Slope (%/year)**	**Intercept**
	+1.18252 ± 0.61220	0.98564 ± 0.00377
1998.38 ± 0.19	–0.39973 ± 0.12559	1.00147 ± 0.00789
2000.06 ± 0.40	+0.26020 ± 0.91255	0.98377 ± 0.02608
2000.56 ± 0.59	–0.24654 ± 0.02038	0.99989 ± 0.03913
2009.74 ± 2.67	–0.15644 ± 0.11282	0.98875 ± 0.04169

Table 14: RMS Values for the L and M Mode TDS Fits.

Mode	RMS (%)
G230LB/2375	0.3
G430L/4300	0.5
G750L/7751	0.2
G230MB/1995	0.4
G230MB/2416	0.5
G430M/3165	0.3
G430M/4194	none, gain problems
G750M/7283	0.05

Proposal ID 12773: MAMA Spectroscopic Dispersion Solution Monitor (PI: Paule Sonnentrucker)

Analysis Lead, Others: Paule Sonnentrucker

Summary of Goals
Constrain STIS MAMA dispersion solutions using internal LINE wavecal data for the E140H, E140M, E230H, E230M, G140L, G140M, G130L and G230M gratings, the 0.2x0.09", 0.2x0.06", 0.1x0.09 and 52x0.1 slits and a total of 17 central wavelengths supported for MAMA spectroscopic observations. There were no external targets used.

Execution
This yearly monitoring executed Oct 17-18, 2011 for a total of 7 orbits, 1 visit each. The data for all grating/cenwave combinations were successfully taken. No data loss occurred.

Summary of Analysis
The LINE lamp exposures were reduced with CalSTIS as if they were science exposures. The emission lines in the resulting x1d spectra were fitted with Gaussian profiles. The difference between the fitted line centroids and the corresponding laboratory wavelengths was computed for all identified lamp lines. For each setting the mean and standard deviation of the latter differences were then calculated.

Accuracy Achieved
The mean of the difference distribution is lower than 0.1 pixel and the standard deviation is lower than 0.33 pixel for the all gratings using the H mode. For the M modes, the difference distribution is less than 0.1 km/s and the standard deviation is lower than 0.35 pixels for most configurations. These results are consistent with those reported pre-SM4 and those reported for Cycle 17 by Pascucci et al. (2010; ISR 2011-V1) and for Cycle 18.

Reference Files Delivered
No new file delivered The solution accuracy has not changed since Cycle 17 or since SM4.

Relevant ISRs:
A multi-cycle ISR is being prepared (Sonnentrucker 2015, in prep).

Continuation Plans
Monitoring program for the MAMA dispersion solutions was carried over to Cycle 20 with Program 13143 for a total of 7 orbits, 1 visit each, as in Cycle 19. The gratings and cenwaves used in Cycle 19 were carried over to the Cycle 20 monitoring program.

Supporting Details
Below find, in form of a series of Figures and Tables, the list of the mean and standard deviations for the difference distributions computed when comparing the measured

emission lines with the laboratory line list. These differences were derived from the monitoring data for selected grating/cenwave combinations listed below.

Table 15: Summary of achieved accuracy. The accuracies achieved in Cycle 19 are consistent with those derived in Cycle 18 and fulfill the requirements for the graintg/cenwave combinations monitored in this program.

Grating-Cenwave	Mean Offset (pix)	Standard Dev (pix)
G140L - 1425	0.01	0.21
G140M - 1218	-0.12	0.35
G230L - 2376	-0.04	0.16
G230M - 1687	-0.26	0.59
- 3055	-0.75	0.16

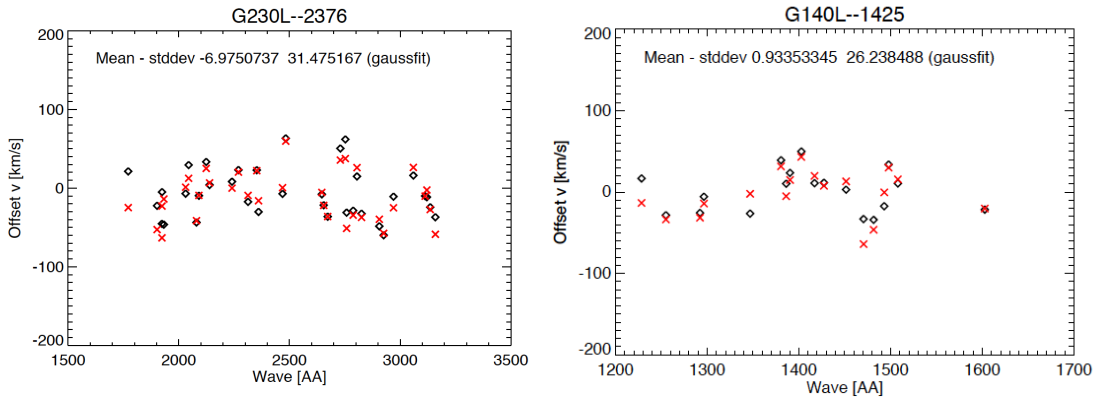

Figure 19: Difference between the fitted line centroids and the corresponding laboratory wavelengths for all identified lamp lines. For each setting the mean and standard deviation of the latter differences were then calculated in velocity space. The black diamonds show results using a Gaussian fit to the lamp emission lines. The red stars show results using a weighted mean centroid fitting. 1 pixel corresponds to 199 km/s for G230L, 16 km/s for G230M, 12 km/s for G140M, and 126 km/s for G140L.

Table 16: Summary of achieved accuracies. The accuracies achieved in Cycle 19 are consistent with those derived in Cycle 18 and fulfill the requirements for the grating/cenwave combinations monitored in this program. 1 pixel corresponds to 1.3 km/s.

Grating-Cenwave	Mean Offset (pix)	Standard Dev (pix)
E140H- 1271	-0.04	0.28
- 1343	0.04	0.16
- 1598	0.04	0.20
E230H- 1763	-0.20	0.19
- 1963	0.03	0.32
- 2713	0.11	0.17

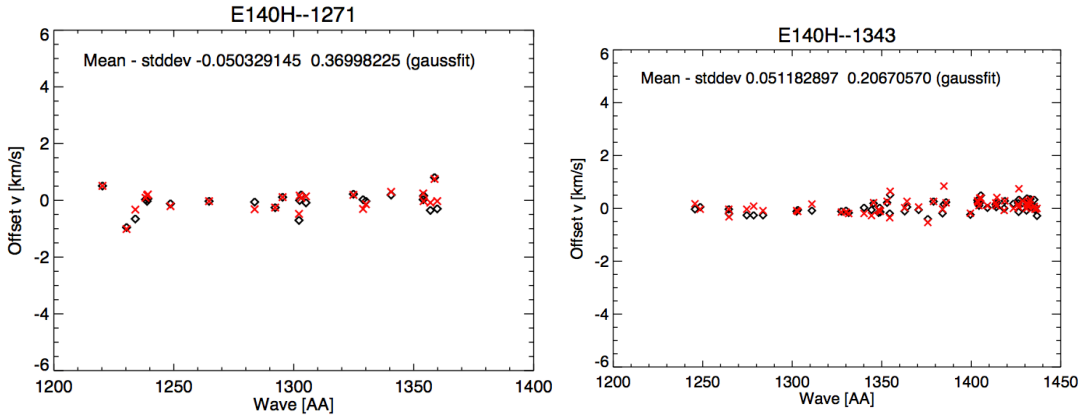

Figure 20: The difference between the fitted line centroids and the corresponding laboratory wavelengths was computed for all identified lamp lines. For each setting the mean and standard deviation of the latter differences were then calculated in velocity space. The black diamonds show results using a Gaussian fit to the lamp emission lines. The red stars show results using a weighted mean centroid fitting. 1 pixel corresponds to 1.3 km/s.

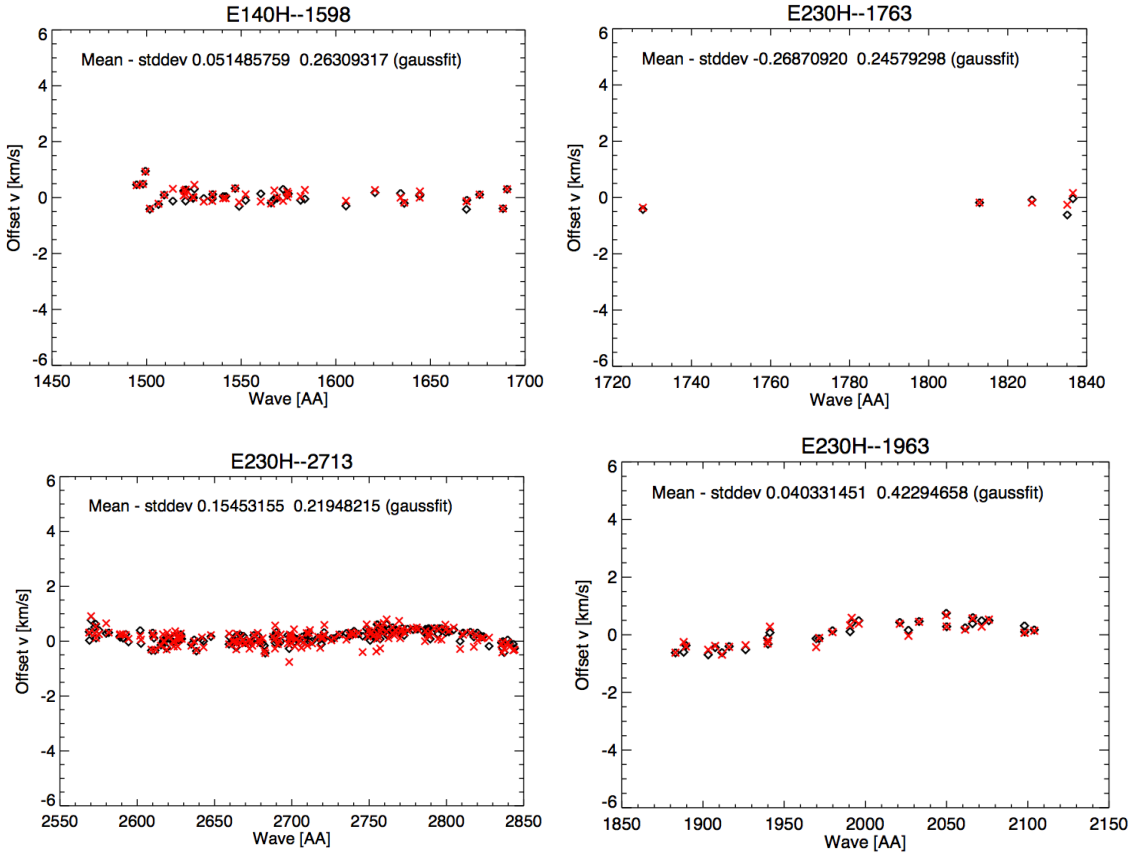

Figure 21: The 4 panels show the difference between the fitted line centroids and the corresponding laboratory wavelengths for all identified lamp lines. For each setting the mean and standard deviation of the latter differences were then calculated in velocity space. The black diamonds show results using a Gaussian fit to the lamp emission lines. The red stars show results using a weighted mean centroid fitting. 1 pixel corresponds to 1.3 km/s.

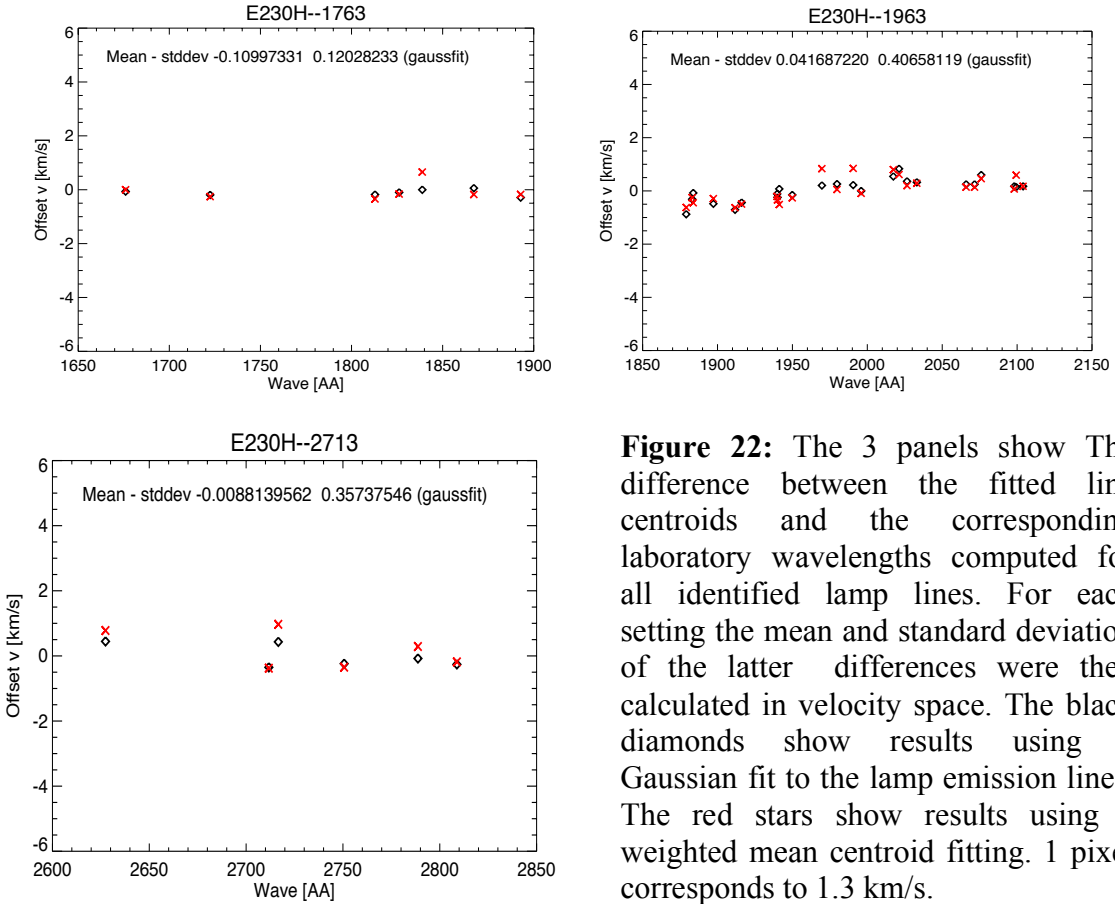

Figure 22: The 3 panels show The difference between the fitted line centroids and the corresponding laboratory wavelengths computed for all identified lamp lines. For each setting the mean and standard deviation of the latter differences were then calculated in velocity space. The black diamonds show results using a Gaussian fit to the lamp emission lines. The red stars show results using a weighted mean centroid fitting. 1 pixel corresponds to 1.3 km/s.

Table 17: Summary of achieved accuracies. The achieved accuracies in Cycle 19 are consistent with those derived in Cycle 18 and fulfill the requirements for the grating/cenwave combinations monitored in this program. 1 pixel corresponds to 3.3 km/s.

Grating-Cenwave	Mean Offset (pix)	Standard Dev (pix)
E140M- 1425	-0.04	0.18
E230M- 1978	-0.08	0.19
- 2415	-0.07	0.44
- 2561	0.06	0.39
- 2707	0.06	0.31

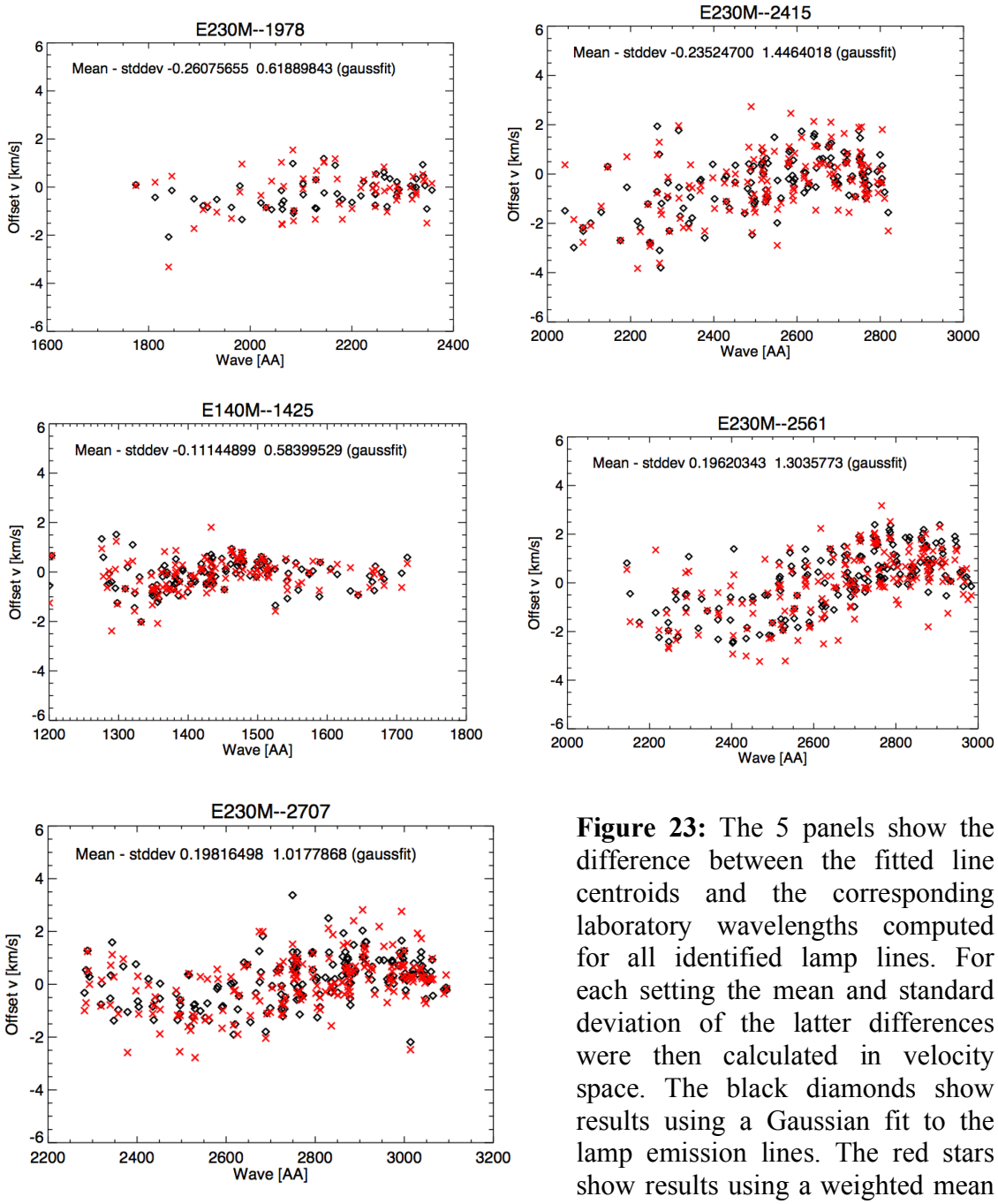

Figure 23: The 5 panels show the difference between the fitted line centroids and the corresponding laboratory wavelengths computed for all identified lamp lines. For each setting the mean and standard deviation of the latter differences were then calculated in velocity space. The black diamonds show results using a Gaussian fit to the lamp emission lines. The red stars show results using a weighted mean centroid fitting. 1 pixel corresponds to 3.3 km/s.

Proposal ID 12774: STIS MAMA Full-Field Sensitivity Monitor (PI: Julia Roman-Duval)

Analysis Lead, Others: Julia Roman-Duval

Summary of Goals: The sensitivity of the STIS MAMAs is observed to decrease linearly with time, with a rate measured from the STIS sensitivity monitors. The TDS trends are thus obtained from spectroscopic observations, and implemented in CALSTIS for both imaging and spectroscopic STIS MAMA observations. The goal of the full-field sensitivity calibration program is to verify that the TDS trends derived from spectroscopic observations are indeed applicable to imaging mode, and correcting the decline in sensitivity in imaging mode accurately.

Execution
Execution occurred as planned on 04-16-2012 between 17:14 and 21:20.

Summary of Analysis
The globular cluster NGC6681 is observed annually as part of the STIS full-field sensitivity calibration program. The NUV images are obtained in the F25SRF2, F25QTZ, and F25CN182 filters, while the FUV images make use of the 25MAMA (clear), F25QTZ, and F25SRF2 filters. Calibrated and geometrically corrected science files (*x2d.fits) for all STIS MAMA full-field sensitivity programs up to Cycle 19 were retrieved from MAST. The data set used in this analysis thus includes programs acquired since 1997 up to 2011 (program IDs: 7080, 7132, 7720, 7788, 8422, 8425, 8858, 8918, 9623, 10032, 11856, 12413, 12774). The NUV and FUV MAMA data are analyzed independently.

All exposures, obtained with different guide stars, show astrometric offsets of ~1". We first register all exposures with the following method. A reference exposure, taken as part of program 11856, is chosen for the NUV (obav01v9q_x2d) and FUV (obav01w4q_x2d). The cross-correlation function of the reference exposure and each exposure of the data set is calculated using the IDL routine CORREL_IMAGES, and its maximum located using the IDL routine CORRMAT_ANALYZE. The location of the maximum of the cross-correlation function corresponds to the shift to be applied to the image to match its astrometry to the reference exposure.

Once all exposures are astrometrically registered to the reference exposure, a catalog of stars is identified in the reference exposure using starfinder. The input parameters of starfinder, such as minimum correlation and detection threshold, were empirically determined via a trial-and-error method. We chose a detection threshold of 10 σ and a minimum correlation of 0.7. Pairs of stars closer than 0.4" were excluded from the catalog. The starfinder point source extraction algorithm requires a PSF to match the shape of point sources to. We derived the PSF directly in each image using a pre-determined list of stars identified by eye. Each star is centroided and stacked with the IDL routine PSF_EXTRACT in order to estimate the PSF.
Our algorithm then performs aperture photometry for each star in the catalog and each

STIS exposure. First, the background, its standard deviation, and the FWHM of the PSF are estimated in each exposure. The typical FWHM of the PSF is 2 pixels. Second, an accurate position for each star in the catalog in each exposure is determined. Due to geometric distortion effects, stellar positions can vary by up to 10 pixels (particularly in the FUV) between exposures, despite the removal of astrometric offsets. Therefore, a test sub-image centered on the position of a star from the catalog, and of width 0.4" is first used to estimate the centroid position of each star in each exposure. Once the centroid position is determined, a second sub-image is extracted of size 0.4" and centered on the previously calculated centroid position. This two-step centering procedure allows us to account for all the stellar flux. Aperture photometry is performed on this sub-image, using an aperture of 5 times the FWHM of the PSF, and annulus also of radius 5 times the FWHM of the PSF, and thickness 5 pixels. The net counts are then converted to magnitudes using the exposure time and the ZMAG keyword populated by CALSTIS, and which includes a correction for the expected TDS trend.

Our algorithm thus provides a catalog of stars and their magnitudes as a function of time, covering the time period 1997-2012. For each star, a linear trend magnitude vs time is fitted (see Figure 24). Figure 25 shows the histogram of the slopes of these trends. The mean weighted slope of the magnitude vs time trend for the NUV-MAMA detector is -0.04 mmag/year, with a standard deviation of 4.19 mmag/year (based on 344 stars). Over 15 years, this represents a change of <1%. For the FUV-MAMA, the mean weighted slope is 0.54 mmag/year (based on 46 stars), with a standard deviation of 3.7 mmag/year. This represents a change of 0.7% over 15 years. Figure 26 shows the time dependency of the full-field sensitivity (expressed as a slope in mmag/year) as a function of magnitude.

Accuracy Achieved
FUV-MAMA: 1%
NUV-MAMA: 1%

Reference Files Delivered
None

Relevant ISRs
STIS ISR 2013-02 (Roman-Duval et al. 2013)

Continuation Plans
Continued in Cycle 20 with no changes as program 13144

Supporting Details
Figures 24, 25 and 26.

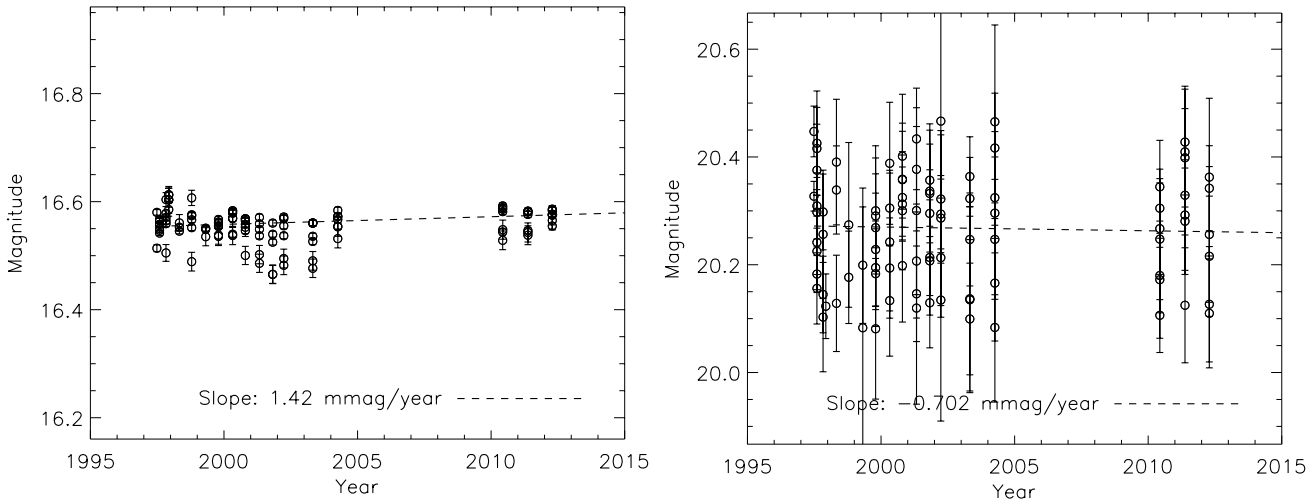

Figure 24: Example of time-dependent full-field sensitivity analysis for a star from the NUV-MAMA star catalog (left) and the FUV-MAMA star catalog (right).

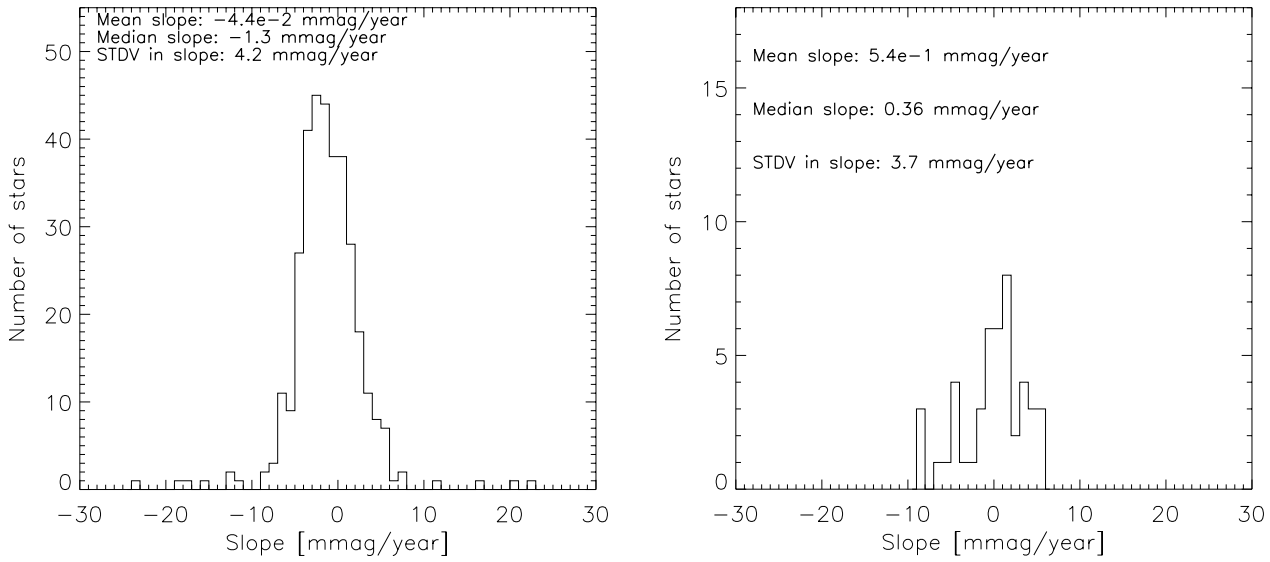

Figure 25: Histrogram of the time dependency of the full-field sensitivity for the NUV-MAMA (left) and FUV-MAMA (right).

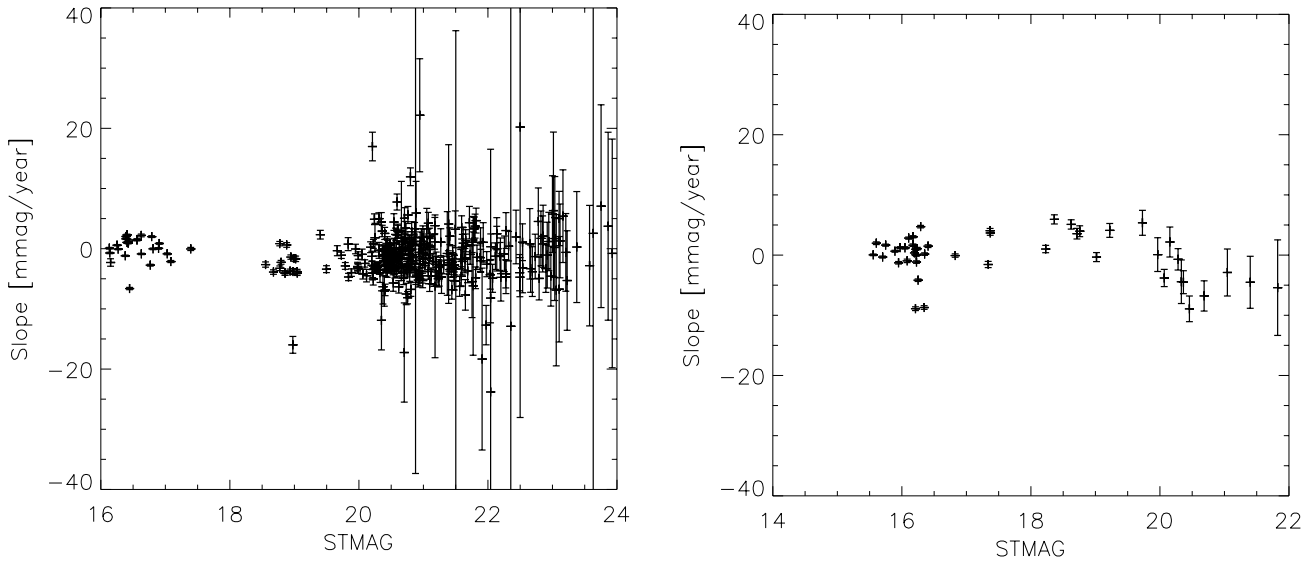

Figure 26: Residual flux calibration error on the imaging mode as a function of magnitude in the NUV-MAMA (left) and FUV-MAMA (right).

Proposal ID 12775: STIS MAMA Spectroscopic Sensitivity, Focus Monitor, and COS Observations of Geocoronal Lyman Alpha Emission (PI: Azalee K. Bostroem)

Analysis Lead, Others: Stephen Holland, Azalee Bostroem, Sean Lockwood

Summary of Goals and program design

The purpose of Program 12775 is to monitor the spectroscopic sensitivity of the STIS MAMAs, monitor the focus, and to observe Geocoronal Lyman Alpha lines with COS. The MAMAs were monitored using the low and medium resolution gratings, and the echelle gratings. The focus was monitored by measuring the full-width at half-maximum (FWHM) on the target acquisition images. We observed the targets listed in Table 18 with the instrument configurations listed in Table 19. The datasets from these observations are also listed in Table 19.

There have been no changes to Program 12775 from Cycle 18.

Execution

Observations were taken several times during the cycle depending on the mode. The number of observations for each mode is listed in Table 19. There were no missed visits and no observatory or pipeline problems with the data from any of the visits.

Summary of Analysis and Results

1. Sensitivity Monitoring

The software used to measure the STIS time-dependent sensitivity (TDS) has been rewritten. The major changes to the software are

- all IDL code has been rewritten in python,
- the number and times of the break points are determined automatically using an F test,
- an error that caused the CTE correction to be sometimes be applied incorrectly was fixed,
- an error in the way that the dark current was computed has been corrected,
- an error that allowed ratios of mis-matched echelle orders was fixed, and
- several consistency checks have been added to ensure that ratios are computed only for data with the same instrument configuration.

The TDS software works by taking the ratio of the flux in each spectrum to the flux in a reference spectrum from early in the STIS mission. A segmented line is fit to these ratios to determine how the STIS MAMA sensitivity has changed over time for each spectral element. The fitting is blind and does not allow for discontinuities in the TDS.

There is no evidence for any change in the TDS trends for any of the L and M modes analyzed for Program 12775. The results for G140L and G230L are presented in Figures 27 and 28, and in Tables 20 and 21. The TDS for the M modes behaves similarly to the corresponding L modes. The behavior of the echelle modes does not follow that of the M or L modes. Their analysis will be documented in a future ISR.

There is no evidence for any drift in the focus from the target acquisition images obtained in Program 12775.

2. Focus Monitoring

We measured the FWHM of the source used for target acquisition in each ACQ image. There is no evidence for any systematic drift in the FWHM values. The complete set of focus measurements are presented in Table 22. The plate scale was 0.050777 arcsec/pix for each observation.

3. Geocoronal Lyman Alpha

The geocoronal Lyman-alpha observations have been archived, but not analyzed.

Accuracy Achieved
Table 23 gives the root mean square (RMS) values for the best-fit segmented lines to the TDS data for each L and M mode. The mean RMS value for the echelle modes is 2.2%, which is approximately five times larger than the mean RMS for the L and M mode. The cause of the large scatter in the echelle modes is under investigation.

Reference Files Delivered
The following synphot reference files for STIS make use of 12775 data and only list the latest delivered versions. They were delivered on Apr 13, 2012.

- stis_ng11_015_syn.fits – FUV/G140L
- stis_ng12_015_syn.fits – FUV/G140M
- stis_ng13_010_syn.fits – FUV/E140M
- stis_ng14_010_syn.fits – FUV/E140H
- stis_ng21_015_syn.fits – NUV/G230L
- stis_ng22_015_syn.fits – NUV/G230M
- stis_ng23_010_syn.fits – NUV/E230M
- stis_ng24_010_syn.fits – NUV/E230H
- stis_nm16_012_syn.fits – FUV/MIRFUV
- stis_nm26_015_syn.fits – NUV/MIRNUV

Relevant ISRs
No ISRs have been published using data from Program 12775.

Continuation Plans
This program is being continued in Cycle 20 as 13145. There were some minor changes for Cycle 20.

- The exposure times for some of the echelle observations have been increased in order to improve the signal-to-noise of the spectra.
- Exposure times, gratings, and central wavelengths for some of the COS parallel observations have been changed.

Supporting Details

Table 18 : Targets for Each Visit.

Visit	Target
L1	GRW+70d5824
L2	GRW+70d5824
L3	GRW+70d5824
M1	AGK+81D266
E1	BD+28D4211
E2	BD+28D4211
E3	BD+28D4211
E4	BD+28D4211

Table 19: Observations and datasets for Program 12775

Spectral Element	Aperture	Wavelength (Å)	Number (visits)	Datasets	Reference Data
MIRROR/ACQ	F28X50LP		8	obw3m1n4q obw3l1efq obw3l2mhq obw3l3fgq obw3e1i3q obw3e2dyq obw3e3dsq	N/A
MIRROR/ACQ/ PEAK	0.1X0.09		3	obw3l1egq obw3l1ehq obw3l2miq obw3l2mjq obw3l3ftq obw3l3fuq	N/A
MIRROR	F28X50OII		1	obw3m1010	
G140L	52X2	1425	3	obw3l1010 obw3l2010 obw3l3010	o3yx14040
G230L	52X2	2376	3	obw3l1020 obw3l2020	o3yx11030

				obw3l3020	
G140M	52X2	1173	1	obw3m1030	o45921020
G140M	52X2	1567	1	obw3m1020	o45902010
G230M	52X2	2818	1	obw3m1040	o45902020
E140M	0.2X0.2	1425	4	obw3e1020 obw3e2020 obw3e3020 obw3e4020	o3zx02080
E230M	0.2X0.2	1978	4	obw3e1030 obw3e2030 obw3e3030 obw3e4030	o8v560040
E230M	0.2X0.2	2707	4	obw3e1050 obw3e2050 obw3e3050 obw3e4050	o8v560050
E140H	0.2X0.2	1416	4	obw3e1040 obw3e2040 obw3e3040 obw3e4040	o45930010
E230H	0.2X0.2	2263	4 (3)	obw3e1010 obw3e2010 obw3e3010 obw3e4010	o4593002
COS/FUV/ G140L	PSA	1105	1	lbw3e4060	N/A
COS/FUV/ G130M	PSA	1291	2	lbw3e1060 lbw3e2060	N/A

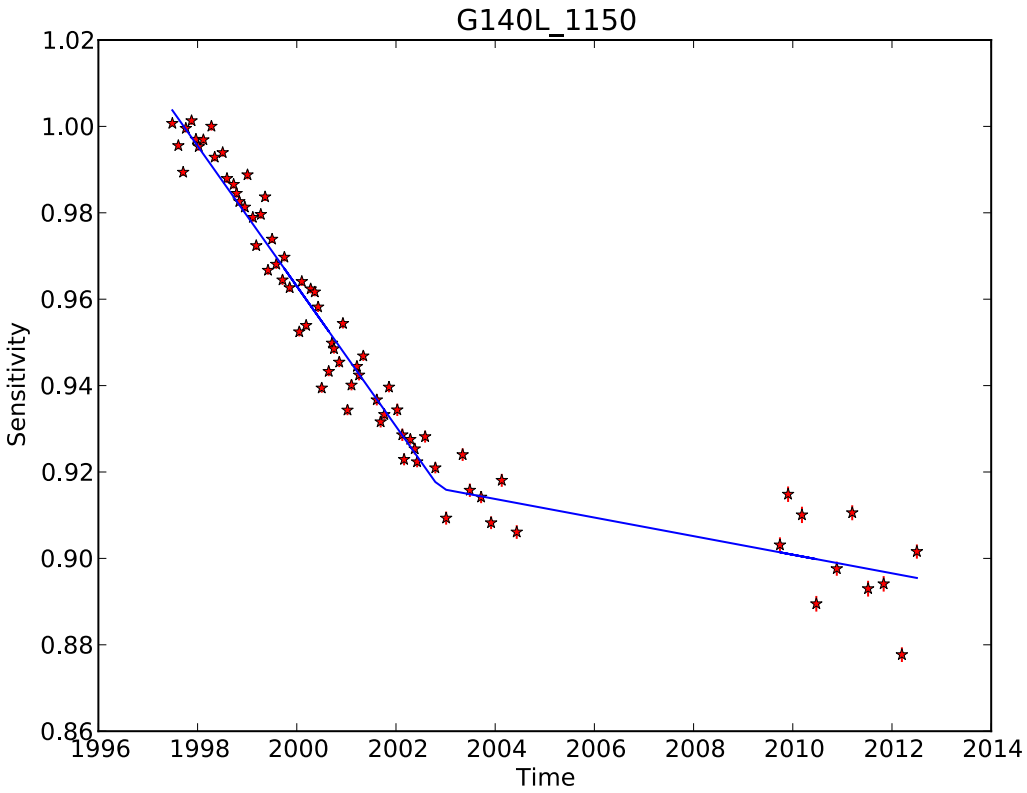

Figure 27: STIS G140L Time-Dependent Sensitivity. The final three data points are from Program 12775. These points show no indication of a change in the TDS decay. The increase in the scatter in the data since 2009 is under investigation.

Table 20: STIS G140L Time-Dependent Sensitivity Parameters

Breakpoint	**Slope (%/year)**	**Intercept**
	–1.62300 ± 0.04989	1.00554 ± 0.00136
2002.89 ± 0.26	–0.21507 ± 0.05501	0.92799 ± 0.00568

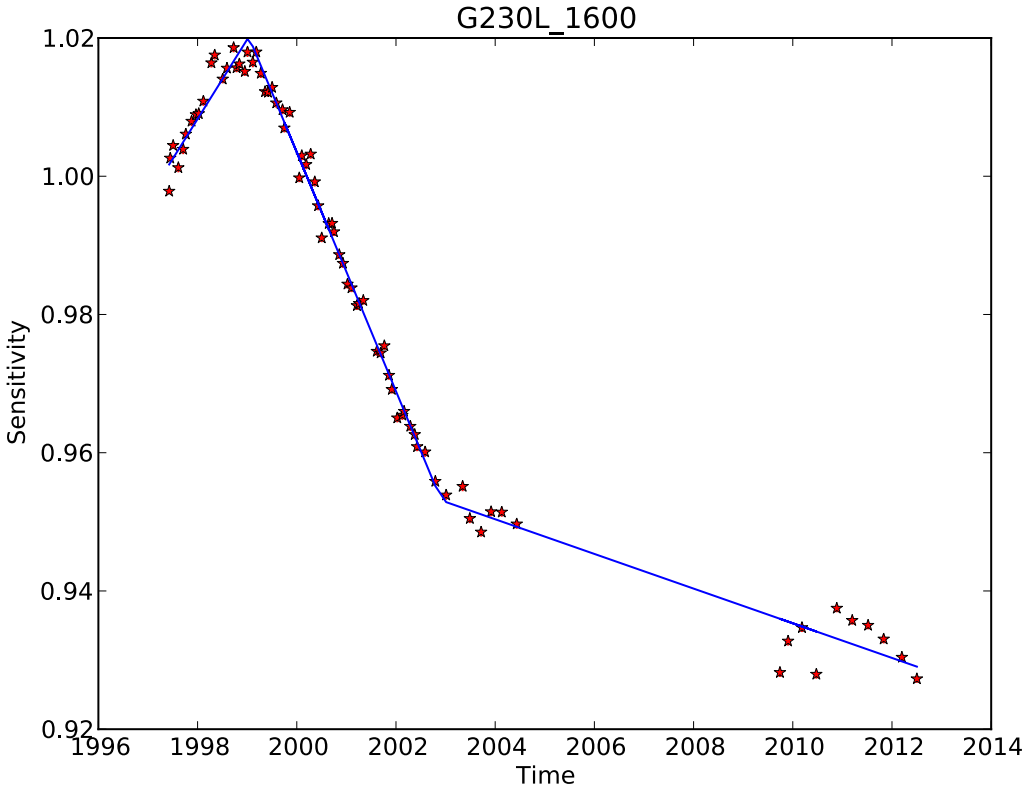

Figure 28: STIS G230L Time-Dependent Sensitivity. The final three data points are from Program 12775. These points show no indication of a change in the TDS decay. The weird behavior since 2009 is under investigation.

Table 21: STIS G230L Time-Dependent Sensitivity Parameters

Breakpoint	**Slope (%/year)**	**Intercept**
	+1.15023 ± 0.09470	1.00116 ± 0.00081
1999.03 ± 0.05	–1.72861 ± 0.03869	1.04876 ± 0.00231
2002.91 ± 0.09	–0.25079 ± 0.01645	0.96698 ± 0.00357

Table 22: FWHM Values (in Pixels) for Each Image Extension in the ACQ Images.

Dataset	**Date**	**FWHM 1**	**FWHM 4**	**FWHM 7**
obw3e1i3q	2011-11-15	1.51	1.61	3.25
obw3e2dyq	2012-01-09	1.64	1.57	3.13
obw3l2mhq	2012-03-14	1.55	1.49	3.19
obw3e3d2q	2012-05-21	1.66	1.54	3.17
obw3l3fgq	2012-07-02	1.41	1.48	3.15
obw3e4wkq	2012-08-09	1.75	1.51	3.13
obw3l1efq	2012-10-31	1.42	1.63	3.14

oc4kl1ykq	2012-11-03	1.61	1.65	3.10
oc4kl1ylq	2012-11-03	1.41	…	…
oc4kl1ymq	2012-11-03	1.43	…	…
obw3m1n4q	2012-11-16	1.41	1.67	3.21
oc4ke1keq	2012-11-17	1.53	1.50	3.21
oc4km1y2q	2012-11-22	1.44	1.59	3.19
oc4ke2ytq	2013-01-10	1.66	1.39	3.12
Mean		1.53 ± 0.03	1.55 ± 0.02	3.17 ± 0.01

Table 23: RMS Values for the L and M Mode TDS Fits.

Mode	**RMS (%)**
G140L/1425	0.6
G230L/2376	0.2
G140M/1173	0.3
G140M/1567	0.7
G230M/2818	0.2

Proposal ID 12776: MAMA Dark Monitor (PI: Colin Cox)

Analysis Lead: Colin Cox

Summary of Goals and program design
This proposal monitors the behavior of the dark current in each of the MAMA detectors, to look for evidence of change in the dark rate, indicative of detector problems developing.

The basic monitor takes two 1300s TIME-TAG darks bi-weekly with each detector. The pairs of exposures for each detector are linked so that they are taken at opposite ends of the same SAA free interval. This pairing of exposures makes it easier to separate long and short term temporal variability from temperature dependent changes.

For both detectors, additional blocks of exposures are taken once a year. These are groups of three 1314s TIME-TAG darks for each of the MAMA detectors, distributed over a single SAA free interval. This provides more information on the brightness of the FUV MAMA dark current as a function of the amount of time that the HV has been on, and gives a better measure of the short term temperature dependence for the NUV MAMA.

Execution
All visits were scheduled as planned and completed successfully.

Summary of Analysis and Results
Each image was analyzed in terms of its mean count rate, the observation time compared to the time of the first observation in the series, and the detector temperature. For the NUV case a detailed model of time and temperature dependence was generated and forms the basis for a proposed new form of calibration table which will capture these dependencies. This has inspired the change of strategy described in the continuation plans with the aim of providing something similar for the FUV case.

Accuracy Achieved
1. NUV MAMA
For a single 1300 second exposure the total number of counts in each pixel is approximately 2000, implying a 2% statistical error on the mean count rate in each indvidual pixel, or about 2 parts in 10^{-5} statistical error in the global rate. The fit to the model gives a RMS deviation of 0.00039 counts per second per pixel for 131 measured points so the mean error is 0.000034 or 1.7% of the typical value of around 0.002 counts per pixel per second.

2. FUV MAMA
A single image contains about 200,000 counts so that the mean rate can be estimated to about 0.2%. Collecting 52 images throughout the year would indicate a cumulative statistical accuracy of 0.03% since there is no obvious long-term variation. However, there is considerable variation of intensity across the image and the value is influenced by how long the MAMA has been turned on, so claiming this accuracy overall would be

unrealistic. From the long term FUV dark rate plot (see Figure 32) it can be seen that the rate varies by at least a factor of 10 from the initial turn-on. However the average value for the full detector settles down to about 10^{-4} counts per pixel per second with a scatter of about 20%. There is a region we have called the glow region, indicated in Figure 31 by the yellow square. Here the rate is about four times the average rate, again with the same initial turn-on behaviour and settling to about 4×10^{-4} counts per pixel per second with about a 20% scatter. The scatter is due to genuine variations rather than measurement errors so it is difficult to quote a traditional error value. There has been no attempt to model this behaviour with the current data, but the strategy for Cycle 20 was aimed at getting a better understanding of the effects of turn-on time and temperature.

Reference Files Delivered

No reference files were delivered to CDBS, but updates in the form of images, text files and plots were placed on the monitor web pages http://www.stsci.edu/~STIS/monitors/nuv and http://www.stsci.edu/~STIS/monitors/fuv

Relevant ISRs

Instrument Science Report STIS 2013-01was published with the title "Dark count rates in the STIS MAMA" (Cox et al. 2013).

Continuation Plans

For Cycle 20 this program was separated into proposals 13147 for the NUV MAMA and 13146 for the FUV. For the NUV a slight scheduling change was made so that the two exposures are taken six hours apart rather than the maximum separation possible. Most observations are taken within six hours of turn-on and so this provides a more suitable dark rate measurement. For the FUV the schedule has been further modified so that in each visit six exposures are taken across a six hour period. To keep within the visit budget these visits only occur every six weeks rather than bi-weekly. This allows a more detailed study of the time and temperature variation of the dark count rate.

Supporting Details

1. NUV MAMA

The long-term variation of the dark rate between November 2010 and the present has been fitted with a double exponential. The deviation from this, driven by detector temperature follows a quadratic function of the temperature. Figure 29 straddles the Cycle 19 period from November 2011 to October 2012 and includes data from Cycles 18 and 20.

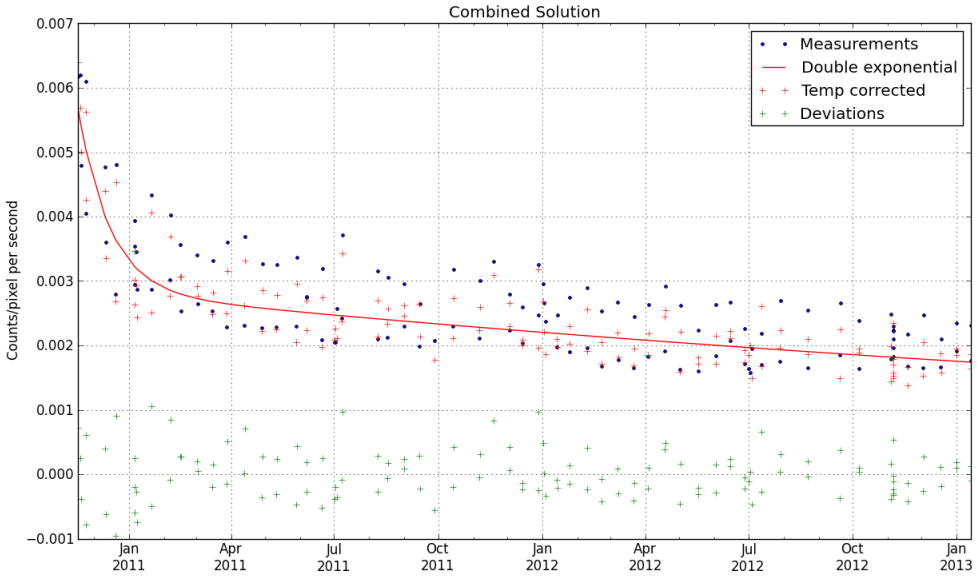

Figure 29: NUV-MAMA dark rate as a function of time, with a exponential fit overalid.

The fit illustrated has a long-term form of:

$$D(t) = 2.84 \times 10^{-3} \exp(-\text{days}/28.8) + 2.9 \times 10^{-3} \exp(-\text{days}/1697.5))$$

Some of the scatter can be explained by the temperature dependence of the dark rate. So to the above formula should be added a quadratic function of the temperature given by

$$S(T) = 4.27 \times 10^{-4} + 4.43 \times 10^{-5} (T-38) - 5.78 \times 10^{-5} (T-38)^2$$

where S(T) is illustrated in Figure 30. Full details are provided in the STIS ISR 2013-01 (Cox et al. 2013).

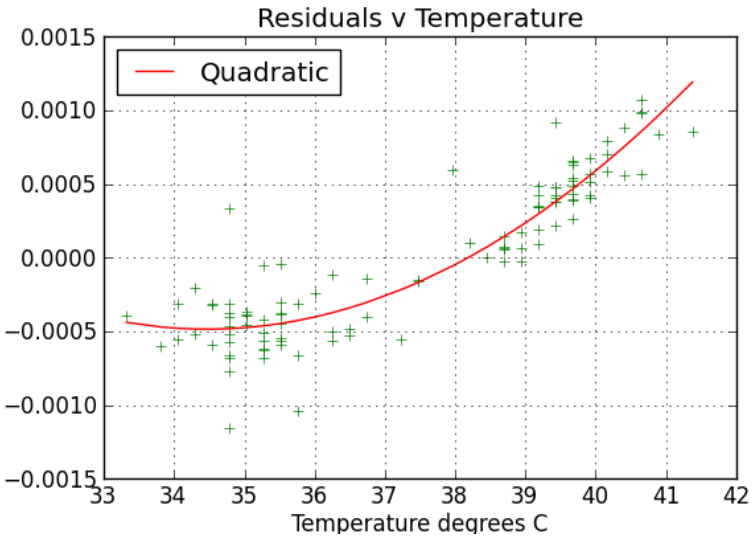

Figure 30: Temperature dependence of the NUV dark rate, with a quadratic fit overlaid.

2. FUV MAMA

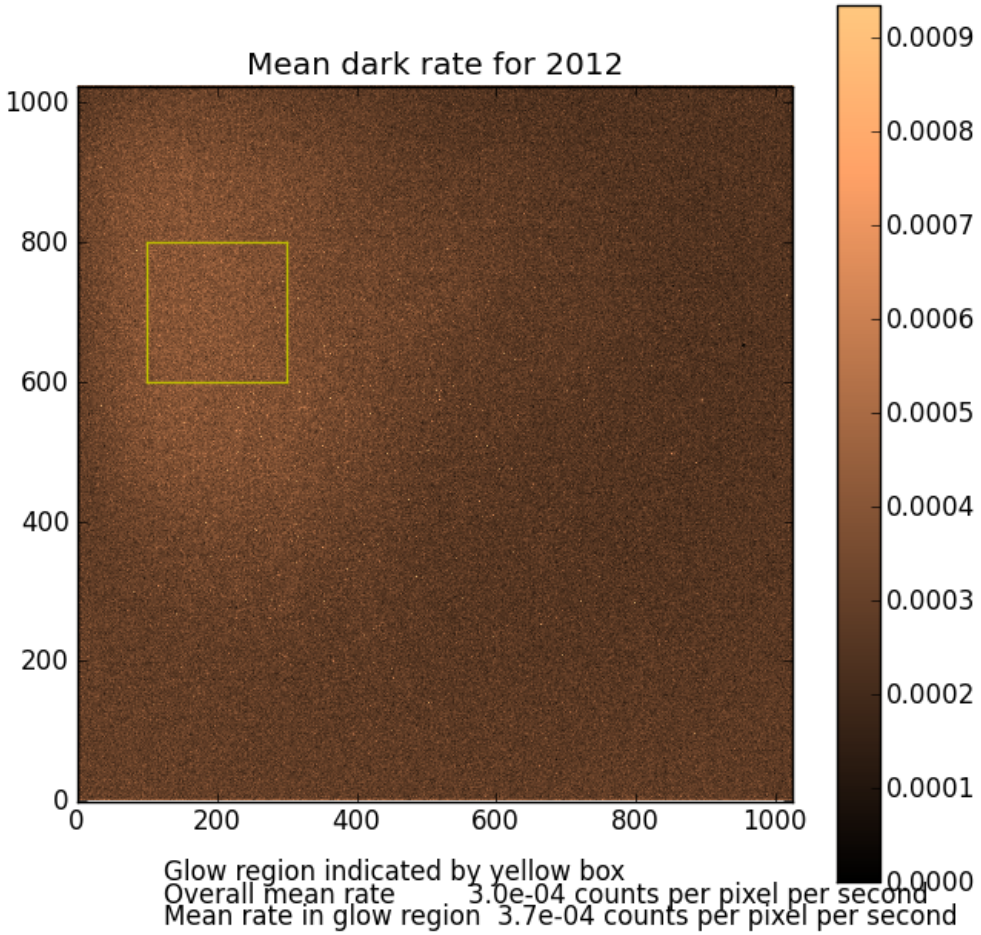

Figure 31: Cumulative image for all data collected in 2012 is shown with the glow region indicated by a yellow rectangle.

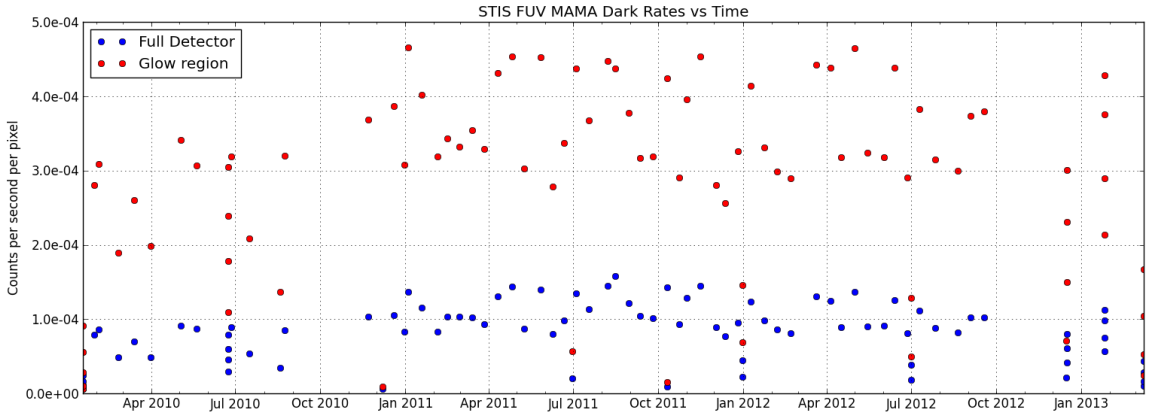

Figure 32 STIS FUV MAMA dark rates from January 2010 to January 2013. No long term variation is discernible. The glow region is about four times as bright as the average.

Proposal ID 12777: STIS MAMA NUV Flats (PI: Elena Mason)

Analysis Lead, Others: Elena Mason

Summary of Goals
This program is aimed at obtaining NUV-MAMA flat-field observations for the construction of pixel-to-pixel flats (P-flats) with a SNR of ~100 per binned pixel. The flats are obtained with the DEUTERIUM lamp and the medium-resolution grating G230M. The choice of central wavelength and slit combination depends on the observed count level within each exposure.

Note that STIS NUV-MAMA flats are taken every other cycle (i.e. during odd number cycles) in order to preserve the remaining DEUTERIUM lamp lifetime. In addition they are taken mainly for monitoring purposes, as there is a limit to how well one can correct the MAMA data.

Execution
We used a total of 11 orbits to collect the desired signal. These were executed in the period October 2011 – February 2012 making sure that the visits were not consecutive in order to limit the lamp usage in the case of a technical failure (e.g. a detector safing without an instrument suspend could prevent data from being collected even though the lamp would still be turned on). The instrument setup adopted during the first visit was the same used in the last exposure of the previous NUV-MAMA monitoring program, i.e. G230M/2338/52X0.5 with exposure time equal to 4630 s. This was done to verify that the count rate is within the safe limits (~250000-280000 cps/frame) and determine which instrument setup to adopt next, should the signal be insufficient. All the subsequent visits were executed adopting the setup G230M/2419/52X0.5 and exposure time of 3588 s, delivering a factor 1.17 more counts per exposure and saving about 2.9 hr of lamp lifetime. In addition five different SLIT-STEP positions were adopted during the program execution in order to uniformly illuminate the whole detector.

All the visits where completed successfully with no failure of any type.

Summary of Analysis
The frames collected within the program were combined and processed using the existing IDL code by Brown et al. (2002, STIS-TIR 2002-03). They were also combined and processed using a PI written script which creates the P-flat by column-by-column and line-by-line fitting of the cumulative data signal with a high (~7-9) order polynomial. The comparison of the two methods has been discussed in the STIS-TIR 2013-01. For flat-field correction of science data only a combination of P-flats obtained with Brown's IDL code should be used.

The P-flat produced within this program is not suitable – alone – as reference file for flat-fielding of science observations. Following Brown et al. (2002) analysis the P-flat from at least 5 different cycles should be combined in a master reference P-flat. We have verified

that using the combined P-flats from cycle 19, 17 and/or cycle 19, 17 and 11, the science reduced data do not reach the same SNR as when flat-fielded with the reference P-flat currently in use (mbj1658do_pfl.fits, produced in 2002). It might be possible to produce a new reference P-flat in the future, once STIS NUV MAMA flats monitoring programs of Cycles 21 and 23 have been completed. However, careful comparison with the reference P-flat currently in use should be performed before its replacement. In addition, it is known (Brown et al. 2002) that there is a limit to how well one can correct the MAMA data, so combining all the existing in-flight flat frames will not deliver higher SNR science data than currently possible.

P-flats were created for Cycles 11, 17 and 19 and compared in order to evaluate possible changes in the detector characteristics. Changes in the pixel-to-pixel response are more difficult to assess as this should be done using higher SNR data (~100 per high resolution un-binned element, in place of the current SNR~50) and with the same instrument setup. Each STIS NUV MAMA flat monitoring program adopted different instrument setups in order to maximize the incoming photon flux and lamp lifetime and did not collect sufficient signal to directly test the pixel-to-pixel response.

Ratios of the P-flats from the three cycles above were made to search for possible detector changes. No significant changes were observed in these ratio images but "spurious" features produced by the non perfect removal of the emission lines (almost vertical structures) and/or by imperfections of the slit edges in combination with the slit reproducibility precision (horizontal structures). We have verified, however, the presence of a residual odd-even effect in the high resolution versions of the ratio images. This residual increases with time and is larger when the Cycle 19 P-flat is compared with the Cycle 11 P-flat (see Table 24 below). The increase of the residual odd-even effect with time was already noted by Brown et al. (2002) and is consistent with previous Brown's et al. conclusions.

P-flat ratio (Cycles)	Residual RMS
11/17	0.040
11/19	0.044
17/19	0.032

Table 24: The standard deviation measured in the area [300:600,600:800] of the ratio images (free from "spurious" features, see text). The first column indicates the cycles whose P-flats are being ratioed. The second column reports the standard deviation as measured in the ratio images.

Accuracy Achieved

The total collected signal during the cycle 19 STIS NUV MAMA flat monitoring delivers the average of 2524 counts per un-binned/high resolution pixel. This corresponds to a SNR of 50 and 100 (assuming Poisson distribution) per high and low (2x2 binning) resolution element respectively and matches the program requirements.

The P-flat obtained following Brown prescription has an average value per high

resolution element (un-binned pixels) of 1 with standard deviation of 0.56. This, by no means should be considered as the accuracy obtained by this program as the STIS MAMA flat pixel value distribution is bi-modal (odd-even column effect) and the measured standard deviation reflects such bi-modality.

Reference Files Delivered
N/A

Relevant ISRs
STIS TIR 2013-01.

Continuation Plans
The STIS NUV MAMA flat monitoring program should continue in Cycle 21 with no significant changes other than the instrument setup “adjustment”, to allow the collection of the required SNR.

Supporting Details
Table 24.

Proposal ID 12778: STIS MAMA Fold Distribution (PI: Thomas Wheeler)

Analysis Lead, Others: Thomas Wheeler, backup: Chris Long

Summary of Goals

The performance of MAMA microchannel plates can be monitored using a MAMA fold analysis procedure that provides a measurement of the distribution of charge cloud sizes incident upon the anode giving some measure of change in the pulse-height distribution of the MCP and, therefore, MCP gain. The goal is to continue monitoring the two STIS MAMA detectors and comparing the results with previous test results to detect trends or anomalous behavior. This proposal is based on Cycle 19 proposal 12778.

Execution

This proposal successfully executed on May 1, 2012.

Summary of Analysis

The engineering telemetry data was examined (voltages, currents, temperatures, relay positions, and status) for agreement with predicted values and previous ground and on-orbit test data. The MAMA engineering telemetry event counter was used to construct a histogram of the number of counts for each fold. The results for each detector are compared and combined with previous test results. Post test, a dark exposure was taken where the counters were cycled and were plotted in a histogram and compared with earlier results.

No anomalous behavior was detected for either MAMA. The NUV MAMA does exhibit a known high dark count rate caused by widow phosphorescence that has been decreasing since SMOV4. Results are sent to the COS/STIS Science Team and V. Argabright of Ball Aerospace for review and comments.

Below are the FUV and NUV fold histograms followed by the post-test dark count histograms.

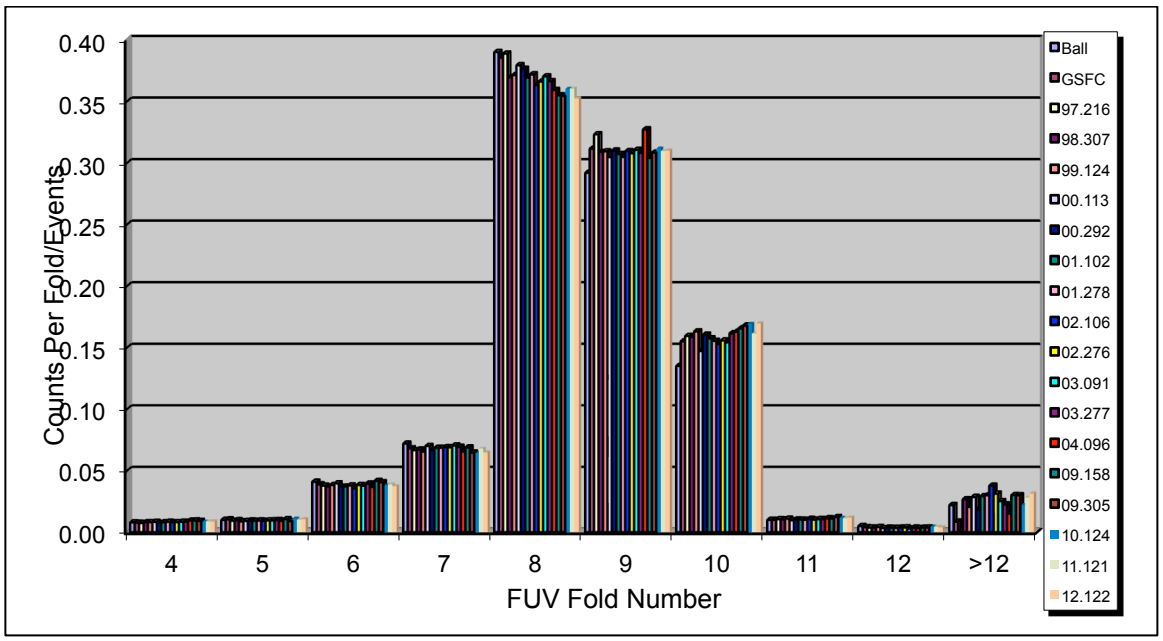

Figure 33. FUV MAMA Fold Histogram

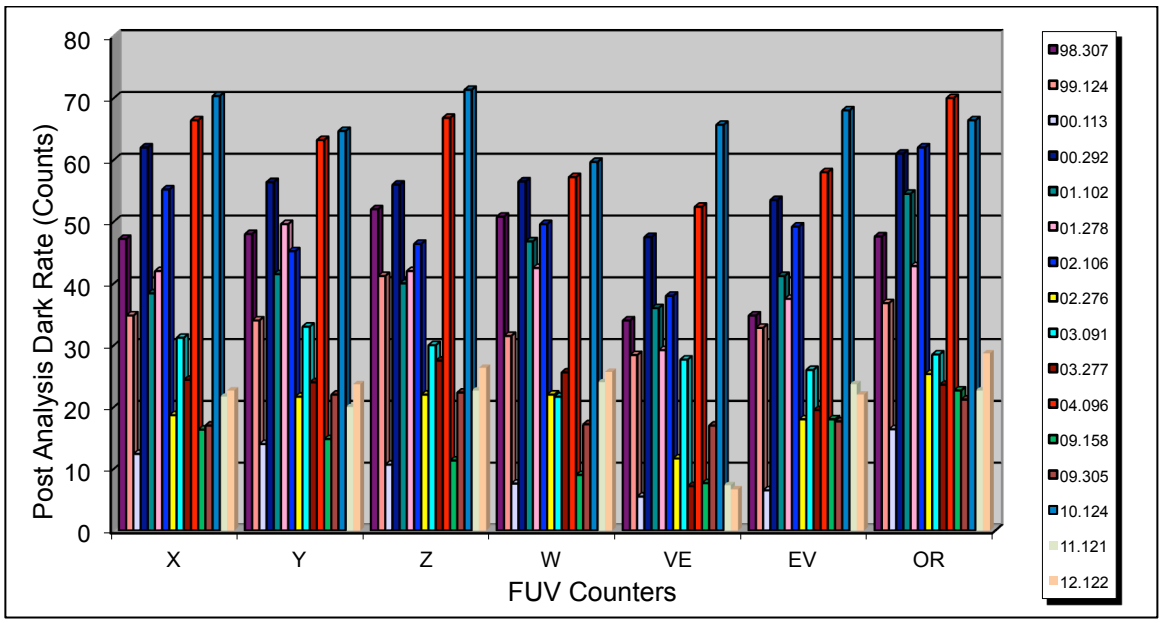

Figure 34. FUV MAMA Post-Test Dark Count Rate

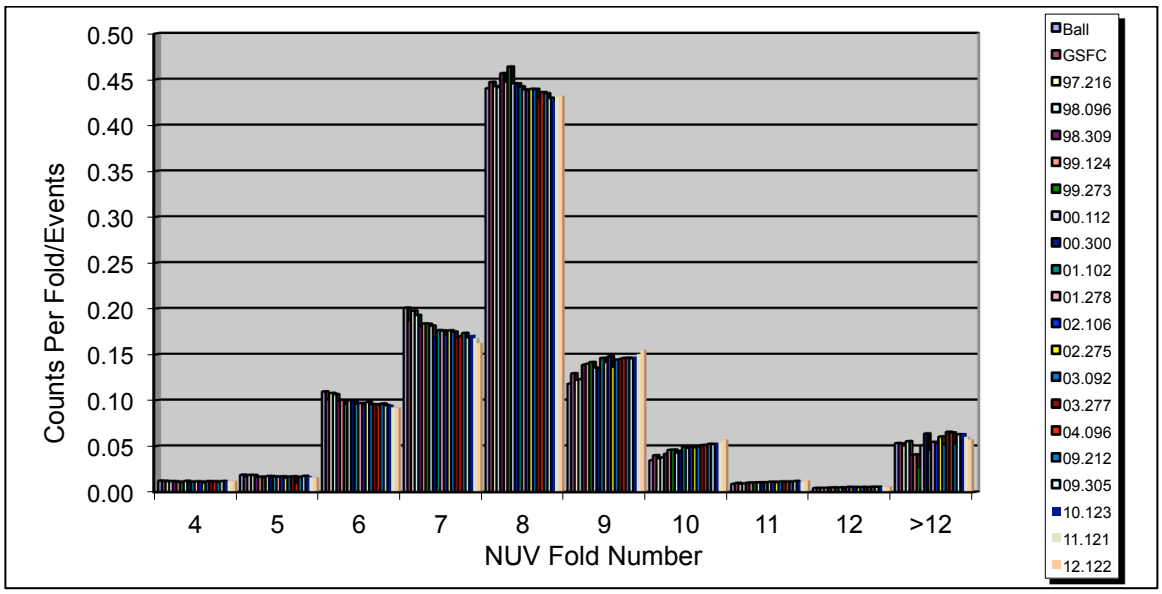

Figure 35. NUV MAMA Fold Histogram

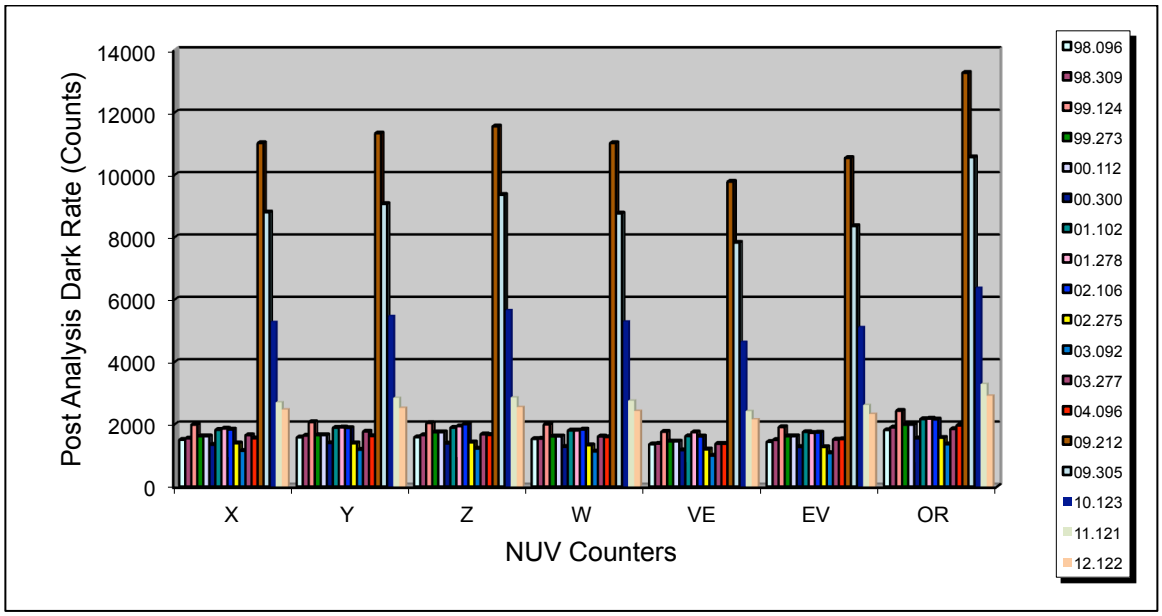

Figure 36. NUV MAMA Post-Test Dark Count Rate

Accuracy Achieved
Position of the peak in the fold distribution can be measured to about 5% accuracy from this procedure.

Reference Files Delivered
N/A

Relevant ISRs
No ISRs will be published.

Continuation Plans
This monitoring program will continue in Cycle 20 with program ID 13149. No modifications are expected.

Supporting Details
See above

Proposal ID 12779: STIS MAMA Recovery after Anomalous Shutdown (PI: Thomas Wheeler)

Analysis Lead, Others: Thomas Wheeler, backup: Chris Long, Alan Welty

Summary of Goals
The goal is verify that the detector has not been damaged and is returned to operations in safe and orderly manner after an anomalous HV shutdown. The recovery procedure consists of three separate tests (i.e. visits) to check the MAMA's health; they must be completed successfully and in order. Diagnostic time-tag images are obtained in tests 2 and 3. This proposal executes the same steps as Cycle 18 proposal 12429. The tests are:

1. Signal processing electronics check
2. Slow, intermediate voltage high-voltage ramp-up where the MCP HV MCP HV is slow- ramped to a voltage 300V below nominal
3. Ramp-up to full operating voltage.

This is followed by and fold analysis test. See STIS ISR 98-02.

Execution
This is a contingency proposal only used in the event of an anomalous HV shutdown and was not executed during Cycle 19.

Summary of Analysis
The analysis is divided into three parts with each part supporting one of the defined tests describe above:

1. Signal processing electronics check. This is the first test of three to recovering a MAMA detector. The purpose is to check out the low voltage power supply and the signal processing chain. An Excel workbook all of the engineering telemetry mnemonics to be examined (voltage, currents, temperatures), the expected values, and the allowable tolerances will be created. A pass/fail column will be defined. Engineering data will be placed into the workbook and compared to expected values.

Next the charge amplifier threshold voltage will be reduced form it nominal value of 0.48 volts to 0.28 volts. This will allow electronic noise to pass through the charge amplifiers and generate events. The number of OR events per seconds will be compared to the expected number +/- a tolerance for a given MAMA tube temperature.

The pass criteria for this test are that engineering telemetry and the expected number of OR counts are within expected values.

The pass criteria for this test are that engineering telemetry is within expected values and no hot spots or unusual features are observed in the science images.

2. The first high voltage ramp-up will be to an intermediate MCP voltage of 300V below the nominal MCP voltage with plateaus. This voltage ramp-up is to condition the high voltage power supply and the MCP. All the engineering telemetry described in step one will be re-examined along with the MCP voltage and current. The MCP voltage +/- a tolerance should be the commanded voltage and the MCP current +/- a tolerance should fit the MCP current model.
The pass criteria for this test are that the engineering telemetry is within expected values and no hot spots or unusual features are observed in the diagnostic science images.

3. The final high voltage ramp-up is to the nominal MCP voltage with voltage plateaus followed by a fold distribution test. This is the last high voltage ramp-up to condition the high voltage power supply and the MCP. All the engineering telemetry described in step one will be re-examined along with the MCP voltage and current. The MCP voltage +/- a tolerance should be the commanded voltage and the MCP current +/- a tolerance should fit the MCP current model.

When the MCP successfully reaches the nominal value, a fold test will be performed. This data will be processed using the "standard fold test analysis tool". The results will be compared to previous fold test results.

The pass criteria for this test are that the engineering telemetry is within tolerance, no hot spots or unusual features are observed in the diagnostic science images and the fold test yields the expected results and show no significant degradation when compared to previous fold tests.

Accuracy Achieved
N/A

Reference Files Delivered
N/A

Relevant ISRs
If an anomalous HV shutdown were to occur, this would be reported in a TIR.

Continuation Plans
This is a contingency proposal. A duplicate proposal will be created for Cycle 20. The proposal ID is 13149. No modifications are expected.

Supporting Details
All relevant turn-on telemetry data will be entered into an Excel similar to SMOV4.

4. Change History for ISR 2014-01

5. References

STIS ISR 98-02, "Cycle-7 MAMA Pulse height distribution stability: Fold Analysis Measurement", H. Ferguson et al.

STIS ISR 2013-01, "Dark count rates in the STIS MAMAs", Cox et al.

STIS ISR 2013-02, "Full-field sensitivity and its Time-dependence for the STIS CCD and MAMAs", Roman-Duval et al.

STIS ISR 2010-91, "Wavelength Calibration Accuracy for the STIS CCD and MAMA Modes", Pascucci et al.

STIS ISR 2009-02, "STIS CCD Performance after SM4: Read Noise, Dark Current, Hot Pixel Annealing, CTE, Gain, and Spectroscopic Sensitivity", P. Goudfrooij et al.

STIS ISR 2013-05 "STIS CCD Spectroscopic P-Flats", E. Mason

6. Appendix

Table 25. Instrument Science Reports & Technical Instrument Reports Produced from Cycle 19 Calibration Programs

Number	Contributing Programs	First Author	Title
STIS TIR 2013-02	12766	Elena Mason	"Revised version of the python code for the creation of STIS CCD P-flats"
STIS ISR 2013-02	12409, 12413	Julia Roman-Duval	"Full-field sensitivity and its time dependence for the STIS CCD and MAMAs"
STIS ISR 2013-01	12415, 12776	Colin Cox	"Dark count rates in the STIS MAMAs"
STIS ISR 2013-05	12776	Elena Mason	"STIS CCD Spectroscopic P-Flats"